nature plants

Article

https://doi.org/10.1038/s41477-024-01642-x

Targeting *Magnaporthe oryzae* effector MoErs1 and host papain-like protease OsRD21 interaction to combat rice blast

Received: 25 July 2023

Accepted: 31 January 2024

Published online: 26 February 2024

Check for updates

Muxing Liu[1,6], Fangfang Wang[2,6], Bo He[1,6], Jiexiong Hu[1], Ying Dai[1], Weizhong Chen[1], Mingxi Yi[1], Haifeng Zhang[1], Yonghao Ye[1], Zhongli Cui[3], Xiaobo Zheng[1], Ping Wang[4], Weiman Xing[5] ✉ & Zhengguang Zhang[1] ✉

Effector proteins secreted by plant pathogenic fungi are important artilleries against host immunity, but there is no precedent of such effectors being explored as antifungal targets. Here we demonstrate that MoErs1, a species-specific effector protein secreted by the rice blast fungus *Magnaporthe oryzae*, inhibits the function of rice papain-like cysteine protease OsRD21 involved in rice immunity. Disrupting MoErs1–OsRD21 interaction effectively controls rice blast. In addition, we show that FY21001, a structure–function-based designer compound, specifically binds to and inhibits MoErs1 function. FY21001 significantly and effectively controls rice blast in field tests. Our study revealed a novel concept of targeting pathogen-specific effector proteins to prevent and manage crop diseases.

Structure-based designing of drugs is traditionally utilized to discover human therapeutic drugs[1] but is rarely used for the discovery of fungicides for crop protection. The main reason is that small molecules with feasible interfering activities or structures of target proteins with novel functions are not easy to obtain. Therefore, examining pathogen–plant interactions to identify unknown interactive mechanisms or antipathogen targets could provide an alternative venue leading to designer antifungal compounds.

During pathogen–host interaction, pathogens secrete effector proteins to play a significant role in pathogenicity. At the same time, plants depend on pathogen-associated molecular-pattern-triggered immunity and effector-triggered immunity to defend themselves against attacking pathogens[2,3]. Effector proteins are known to exhibit a pattern of rapid evolution with instability and variability, leading to their limited significance as potential targets of fungicides[4,5]. However, whether species-specific effector proteins could be targeted for fungicidal effect is unknown. We answer this question by exploring species-specific and evolutionarily conserved effector proteins as potential fungicidal targets.

Magnaporthe oryzae causes one of rice's most devastating diseases, the rice blast, which accounts for 10–30% of the world's annual rice loss. This is equivalent to the food ration of ~60 million people annually[6,7]. In general, rice blast is managed by applying an array of fungicides, including sterol demethylation inhibitors, mitochondrial respiration inhibitors and melanin biosynthesis inhibitors[8–10]. However, due to the fast emergence of fungicide resistance and environmental concerns, the development of novel fungicides against new targets is particularly urgent[8].

An increasing body of evidence suggests that papain-like cysteine proteases are central hubs in plant immunity[11–15]. For successful colonization, pathogens secrete effector proteins to overcome such an immunity[11,12,16–22]. How effectors and their target interactions are explored for disease control remains to be seen. Here we examined the interaction between *M. oryzae*-specific effector MoErs1 and the host

[1]Department of Plant Pathology, College of Plant Protection, Nanjing Agricultural University, and Key Laboratory of Integrated Management of Crop Diseases and Pests, and Key Laboratory of Plant Immunity, Ministry of Education, Nanjing, China. [2]Shanghai Key Laboratory of Regulatory Biology, Institute of Biomedical Sciences and School of Life Sciences, East China Normal University, Shanghai, China. [3]College of Life Science, Nanjing Agricultural University, Nanjing, China. [4]Departments of Microbiology, Immunology and Parasitology, and Pediatrics, Louisiana State University Health Sciences Center, New Orleans, LA, USA. [5]Shanghai Key Laboratory of Plant Molecular Sciences, College of Life Sciences, Shanghai Normal University, Shanghai, China. [6]These authors contributed equally: Muxing Liu, Fangfang Wang, Bo He. ✉e-mail: weimanxing@shnu.edu.cn; zhgzhang@njau.edu.cn

papain-like cysteine protease. We also designed the small-molecule compound FY21001 that targets MoErs1 to inhibit its papain-like cysteine protease-suppressing function. Finally, we showed that the application of FY21001 effectively manages rice blast.

Results

M. oryzae secretes effector MoErs1 to inhibit rice immunity

In previous studies, we found that the Qc-soluble *N*-ethylmaleimide-sensitive factor attachment protein (Qc-SNARE) MoSyn8 mediates intracellular trafficking in *M. oryzae*[23]. To examine how MoSyn8 might affect effector secretion, secreted proteins were extracted from the Δ*Mosyn8* mutant and wild-type Guy11 strains cultured for 4 days in liquid nitrogen starvation minimal medium (MMN), which induces protein secretion during the early infection process[24–26]. Following separation by two-dimensional electrophoresis (2D-E), we performed comparative secretome analysis and successfully identified proteins encoded by 12 genes (Supplementary Fig. 1 and Table 1). We then obtained knockout mutants for 8 of the 12 genes, including *MoERS1* (Effector 1 Regulated by MoSyn8).

MoERS1 is predicted to encode a protein of 214 amino acid residues with an N-terminal signal peptide (SP) (GenBank accession no. OK562582) (Supplementary Fig. 2). To confirm the secretion of MoErs1, the native promotor-driven *MoERS1-FLAG*, the control apoplastic effector *SLP1-FLAG* and the control *GFP-FLAG* fusion genes were generated and transformed into Guy11. Secreted proteins were collected from cultures grown in complete liquid medium (CM), MMN and rice leaves infected with *M. oryzae* at 48 h and analysed using sodium dodecyl sulfate–polyacrylamide gel electrophoresis (SDS–PAGE). MoErs1 and Slp1 were detected in cultures of MMN and infected leaves but not in CM (Supplementary Fig. 3a), suggesting that MoErs1 is secreted during infection.

The expression pattern of *MoERS1* during various growth stages was examined using real-time quantitative PCR (qPCR). *MoERS1* transcripts were significantly higher during mycelial growth, 24-, and 36-h post inoculation (hpi), which is different from observations in well-characterized effectors, such as Bas4 and AvrPi9 (Supplementary Fig. 3b)[27,28]. We then characterized the phenotype and virulence of MoErs1 using one of the three independent Δ*Moers1* knockout mutants exhibiting a similar phenotype (Supplementary Fig. 3c). The Δ*Moers1* mutant was moderately reduced in vegetative growth, but conidia formation, germ tube growth and appressorium formation were the same as those in Guy11 and the complemented Δ*Moers1/MoERS1* strain (Supplementary Table 2). Intriguingly, in conidial suspension spray assays, a drastic reduction of disease severity was observed, as lesion area and fungal DNA were decreased by >60% on leaves infected with the Δ*Moers1* mutant compared with controls (Fig. 1a–c). Specifically, necrotic lesions caused by the Δ*Moers1* mutant failed to produce any conidia, whereas the typical disease lesions caused by Guy11 and the complemented strain produced abundant conidia (>80%, $n = 100$) (Fig. 1d,e). These results indicate that MoErs1 plays a role in vegetative growth and this role becomes significant in virulence.

To examine the secretion of MoErs1 in rice cells, a native *MoERS1* promoter-driven *MoERS1-RFP* fusion gene was generated and transformed into the Δ*Moers1* and Δ*Mosyn8* mutants, respectively. The observation of ~100 infectious sites showed over 70% of sites with red fluorescence accumulation in the biotrophic interface complex of the Δ*Moers1* mutant but not the Δ*Mosyn8* mutant (Fig. 1f). In addition, the native promoter-driven *MoERS1-RFP* with a nuclear localization signal (MoErs1-RFP-NLS) and Slp1-GFP fusion genes were generated and co-transformed into the Δ*Moers1* mutant. Red fluorescence was found in the biotrophic interface complex and the nuclei of host cells invaded by the complemented strain, while green fluorescence was readily detected in the extra-invasive hyphal membrane that has no detectable red fluorescence (Fig. 1g). We also found that Brefeldin A (BFA) treatment did not affect the localization of MoErs1, in contrast to Slp1 (Fig. 1g). These observations indicate that MoErs1 is a secreted cytoplasmic effector protein required for pathogenicity.

To explore how MoErs1 contributes to pathogenicity, we performed infection assays on rice sheaths. The results showed that invasive hyphae growth was significantly restricted at 24 hpi in the Δ*Moers1* mutant (>85%, $n = 100$) and the invasive hyphae failed to expand to adjoining cells even at 48 hpi (>80%, $n = 100$) (Supplementary Fig. 4a), indicating the function of MoErs1 in invasive growth and lesion formation.

To examine whether MoErs1 inhibiting the host immune response is associated with the rapid production of reactive oxygen species (ROS), we used 3,3′-diaminobenzidine (DAB) staining to estimate ROS production in infected rice sheaths. ROS was rarely found in infection by Guy11 and the complemented strain, but was readily detected in cells infected with the Δ*Moers1* mutant (Supplementary Fig. 4b,c). We also pretreated the rice sheaths with diphenyleneiodonium, an inhibitor of NADPH oxidases involved in ROS production[29], and observed invasive hyphae growth of ~100 appressorial penetration sites by rating the hyphal growth from levels I to IV (Supplementary Fig. 4d). The results showed that the invasive hyphae of the Δ*Moers1* mutant could usually expand, similar to those of Guy11, at 24 and 48 hpi (Supplementary Fig. 4e). We then generated transgenic rice lines overexpressing signal peptide-less MoErs1 (*MoERS1*$^{\Delta SP}$-OX) in the TP309 background. The *MoERS1*$^{\Delta SP}$-OX rice lines were more susceptible to rice blast and the Δ*Moers1* mutant was as virulent as Guy11 with typical lesions (Supplementary Fig. 5a–f). Transgenic rice lines overexpressing *MoERS1* were as susceptible as the wild-type TP309 to *Bipolaris oryzae* and *Xanthomonas oryzae* (Supplementary Fig. 5g,h). These data indicate that MoErs1 has a critical role in suppressing host immunity.

To further examine whether the deletion of *MoERS1* results in a defect in effector secretion, the AVR-Pia and AVR-Piz-t genes fused with a C-terminal GFP were expressed in the Δ*Moers1* and Guy11 strains. Both strains expressing Avr-Pia or Avr-Piz-t failed to produce any lesions on LTH-Pia (Pia R gene monogenetic rice line) and LTH-Piz-t (Piz-t R gene monogenetic rice line) rice lines (Supplementary Fig. 6a,b), indicating that MoErs1 does not interfere with the recognition of Pia/Avr-Pia and Piz-t/Avr-Piz-t.

Fig. 1 | MoErs1 is a cytoplastic effector required for the virulence of *M. oryzae*. **a**, MoErs1 is required for the virulence of *M. oryzae*. Conidial suspensions (5×10^4 conidia per ml in 0.2% gelatin) of Guy11, Δ*Moers1* mutants (#1, #7 and #18) and the complement strains were sprayed onto 2-week-old rice seedlings (CO39). Diseased rice leaves were photographed after 7 days post inoculation (dpi). **b**, Fungal growth measured by quantifying *M. oryzae* genomic 28S rDNA relative to rice genomic Rubq1 DNA. Mean ± s.d. of 3 determinations. Significant differences were determined using two-sided Duncan's new multiple-range tests and marked with different letters. **c**, The disease lesion area (DLA) was assessed using Image J software. The biologically independent DLA is displayed as boxes with individual datapoints ($n = 9$). The error bars represent maximum and minimum values. Centre line, median; box limits, 25th and 75th percentiles. Significant differences were determined using two-sided Duncan's new multiple-range tests and marked with different letters. **d**, The Δ*Moers1* mutant cannot produce typical lesions on rice leaves. Conidiation lesions on surface-sterilized rice leaves in **a** were counted and photographed. The lesions producing conidia (left) are typical lesions and the lesions that fail to produce conidia (right) are necrotic lesions. **e**, Statistical analysis of typical and necrotic lesions on rice leaves in **a**. **f**,**g**, MoErs1 is a cytoplasmic effector regulated by MoSyn8 (**f**). The fungal transformants Δ*Moers1* and Δ*Mosyn8* expressing MoErs1:RFP or MoErs1:RFP:NLS/Slp1:GFP at 30 hpi in the sheath cells of rice cultivar CO39 treated with or without Brefeldin A (BFA) are shown as a projection under a confocal microscope, the left column is RFP, the middle is DIC, and the right is Merge (**g**). The experiments were repeated independently at least 3 times with similar results. Arrows indicate the biotrophic interface complex and the white asterisks indicate rice nuclei. Scale bar, 10 μm.

https://doi.org/10.1038/s41477-024-01642-x

We further observed the localization of Avr-Pia and Avr-Piz-t in the Δ*Moers1* mutant and Guy11 strains during infection and found that GFP was normally present in the biotrophic interface complexes of both strains (>80% of 100 imaged infection sites) (Supplementary Fig. 6c,d). We then observed the localization of the apoplastic effector Slp1 (ref. 30). GFP was readily detected in the extra-invasive hyphal membrane of the Δ*Moers1* and Guy11 strains (>85% of 100 imaged infection sites) (Supplementary Fig. 6e). These data suggest that MoErs1 suppresses host immunity independent of other effector protein secretion.

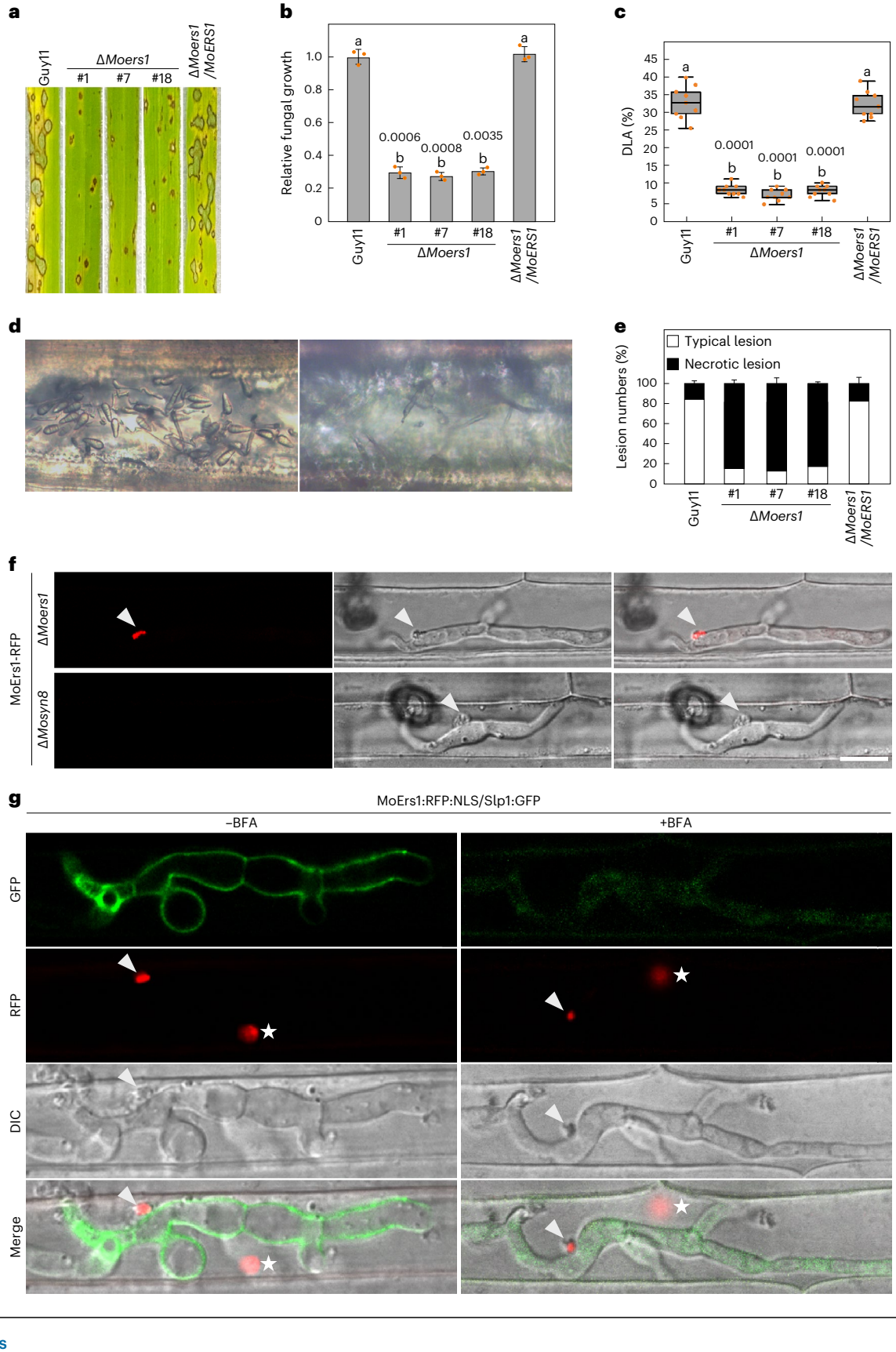

https://doi.org/10.1038/s41477-024-01642-x

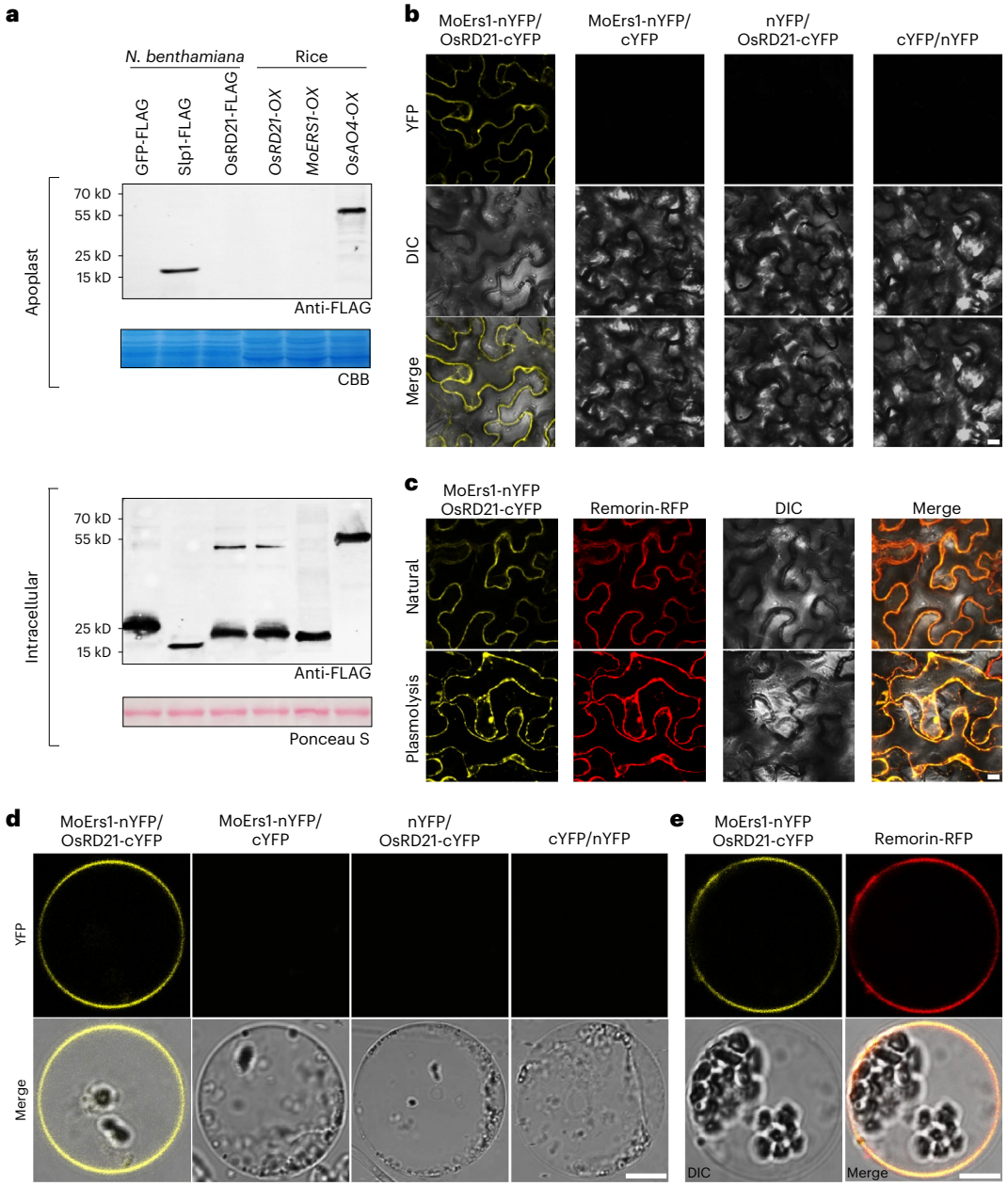

Fig. 2 | MoErs1 interacts with OsRD21 in the plasma membrane in vivo. **a**, OsRD21 is mainly concentrated in intracellular components but not in the apoplast. GFP-FLAG, Slp1-FLAG and proOsRD21-FLAG were transiently expressed in *N. benthamiana*. The *proOsRD21* and *MoERS1* gene-overexpressing rice lines (*OsRD21*-OX and *MoERS1*$^{\Delta SP}$-OX) with a C-terminal FLAG tag were used to determine the distribution of OsRD21 in rice cells; the *OsAO4*-OX overexpressing rice line was used as a positive control[36]. The apoplastic and intracellular leaf extracts were separated and stained with CBB. Immunoblots with appropriate anti-FLAG antibodies showed apoplast Slp1 and OsAO4 levels, but not GFP or OsRD21 levels. **b**,**c**, BiFC assay in *N. benthamiana* (**b**). Co-expression of MoErs1$^{\Delta SP}$-nYFP and proOsRD211-cYFP with a PM marker Remorin-RFP, treated with (plasmolysis) or without (natural) 1 M NaCl (**c**) showed that MoErs1 and OsRD21 co-localized in the PM. The relevant negative controls in **b** showed no fluorescence. Scale bar, 5 μm. **d**,**e**, BiFC assays in rice protoplast cells (**d**). Co-expression of MoErs1$^{\Delta SP}$-nYFP and proOsRD211-cYFP with Remorin-RFP (**e**) showed that MoErs1 and OsRD21 co-localized in the PM in rice protoplasts. The relevant negative controls in **d** showed no fluorescence. Scale bar, 10 μm. All experiments were repeated independently at least 3 times with similar results.

MoErs1 functions as a protease inhibitor that targets OsRD21

To understand MoErs1 functional mechanisms, we determined the crystal structure of MoErs1 at 2.5-Å resolution. MoErs1 was first overexpressed in *Escherichia coli* BL21 (DE3) and purified. The structure of MoErs1 was resolved using the single-wavelength anomalous diffraction method[31]. The model was then refined with R_{work} and R_{free} values of 21.6% and 25.0% (Supplementary Table 3). The final model of MoErs1 contains one MoErs1 in the asymmetric unit (PDB: 7VS2). MoErs1 adopts a typical β-trefoil fold where strands 2, 3, 4, 11, 12 and 13 form a β-barrel covered by 3 2-stranded antiparallel β-sheets (Supplementary Fig. 7a). The disulfide bond between C42 on the short α-helix and C105 on β-strand 5 plays a critical role in the overall rigidity of the MoErs1 structure (Supplementary Fig. 7a,b), which helps the short α-helix to fold back and allows the short helix and β-strand 1 to lean on the surface of the β-barrel. The β-trefoil fold is often found in Künitz-type protease inhibitors[32]. However, structural similarity search using Dali[33] yielded the best match with the Künitz-type protease inhibitor and water-soluble chlorophyll protein (WSCP) at a root-mean-square Ca deviation (RMSD) of 3.4 Å (Supplementary Fig. 7c). These results indicate that MoErs1 might function as an inhibitor of plant-origin proteases.

Brassicaceae WSCP (PDB: 5HPZ) inhibits the activity of *Arabidopsis thaliana* papain-like cysteine protease (PLCP) AtRD21[34,35]. To test whether MoErs1 exhibits proteinase inhibitor activities similar to *Brassicaceae* WSCP, we searched the *Oryza sativa* L. database for AtRD21 homologues and identified a gene locus (LOC_Os04g57440.1) that we named *OsRD21*. OsRD21 has the highest sequence identity and the closest evolutionary relationship with AtRD21 (Supplementary Fig. 8).

RD21s are multicellular organelle localized proteins accumulated in the vacuole and endoplasmic reticulum (ER) bodies[36], and also in the plasma membrane (PM) and apoplastic spaces[11]. To determine the localization of OsRD21, the GFP-tagged full-length OsRD21 was transiently expressed in *Nicotiana benthamiana* and the rice protoplast. The green fluorescence was naturally concentrated on the cell periphery and ER in *N. benthamiana* (Supplementary Fig. 9a,b). When plant cells were treated with a high concentration of salt leading to plasmolysis, fluorescence remained localized at the PM. In addition, OsRD21-GFP co-localized with RFP-tagged Remorin (StREM1.3), an inner PM-localized protein[37,38], and RFP with a signal peptide and ER retention signal HDEL, when they were co-expressed in *N. benthamiana* (Supplementary Fig. 9a,b). We also observed punctae distributed along the PM, hence OsRD21-GFP might localize on vesicles, microdomains or other subcellular components in *N. benthamiana* (Supplementary Fig. 9a,b). However, in the rice protoplast, OsRD21-GFP co-localized with Remorin-RFP on the PM without showing any ER localization (Supplementary Fig. 9c). We also showed that GFP-tagged MoErs1 without the signal peptide localizes to the cytoplasm of the rice protoplast (Supplementary Fig. 9d). All of these tagged proteins can be normally expressed in planta (Supplementary Fig. 9e).

To test whether OsRD21 is secreted into the apoplast, the FLAG-tagged GFP (a negative control), the apoplastic effector Slp1 (a positive control) and proOsRD21 were transiently expressed in *N. benthamiana*. Apoplastic and intracellular leaf extracts were separated and immunoblotted with the anti-FLAG antibody. We found that OsRD21 accumulates in intracellular compartments but not in the apoplast. We also confirmed this result in transgenic rice lines overexpressing *proOsRD21:FLAG* (*OsRD21*-OX) driven by the actin1 promoters, *MoERS1*$^{\Delta SP}$-OX and *OsAO4*-OX (Fig. 2a)[39]. These data indicate that OsRD21 mainly localizes in the PM rather than in the apoplast.

We then examined and verified whether MoErs1 interacts with OsRD21 by carrying out yeast two-hybrid (Y2H), co-immunoprecipitation (co-IP) and bimolecular fluorescence complementation (BiFC) assays of proteins transiently co-expressed in *N. benthamiana* (Fig. 2b,d and Supplementary Fig. 10a,b). To further examine the location of MoErs1–OsRD21 interaction, MoErs1 tagged with N-terminal YFP (MoErs1-nYFP) and OsRD21 tagged with C-terminal YFP (OsRD21-cYFP) were co-expressed with Remorin-RFP in *N. benthamiana* and the rice protoplast. Results indicate that the interaction mainly occurs in the PM (Fig. 2c,e).

MoErs1 inhibits the activity of OsRD21 to promote virulence

To identify the amino acids of MoErs1 required for binding to OsRD21, molecular modelling and docking analysis were carried out. The OsRD21 3D model closely resembles that of barley EP-B2 (PDB ID: 2FO5)[40]. In addition, this result closely aligns with that obtained from alphafold2 calculations, which displayed an RMSD value of 0.545 (Supplementary Fig. 11). ClusPro was used to predict the interactions between MoErs1 loop2 (L2, red), loop4 (L4, chocolate), loop8 (L8, magenta) and β-strand 11 (β11, blue) with OsRD21 (Fig. 3a)[41]. Specifically, L2 (Ser64, Glu67, Phe71 and Pro72) of MoErs1 is predicted to intrude into the active site region of OsRD21 containing Cys165 and His302, thereby blocking its proteolytic activity[34]. Moreover, Ser64 and Glu67 in L2 are predicted to form hydrogen bonds with Gln201 and Ser299 of OsRD21, respectively (Fig. 3a). We also predict that Arg178 and Asp180 in β11, Arg95 in L4 and Gln160 in L8 form hydrogen bonds (yellow dotted line) or non-covalent binding forces (orange dotted line) with Gln201, Asn202, Asp235 and Arg295 of OsRD21, respectively (Fig. 3a). Together, these hydrogen bonds and non-covalent binding forces may stabilize the observed MoErs1–OsRD21 interaction.

To verify this modelling prediction, alanine substitution in each of the four regions was carried out, and Y2H and co-IP assays revealed that mutations in L2 (positions 64, 67, 71 and 72) and β11 (positions 178 and 180) nearly abolished the MoErs1–OsRD21 interaction. In addition, L4 (position 95) and L8 (position 160) are also required for full binding activities (Supplementary Fig. 10a,b). Finally, a microscale thermophoresis (MST) assay and measurement of dissociation constants (K_d) revealed that MoErs1 binds more tightly to OsRD21 than any of its mutated variants (Supplementary Fig. 10c).

To investigate whether MoErs1 inhibits the activity of OsRD21 through binding, we transiently co-expressed MoErs1-GFP and its mutants with the ProRD21-FLAG in *N. benthamiana*. PLCP activity assessments using the previously established method[42] showed that MoErs1 inhibits the activity of OsRD21 more strongly than MoErs1^{L2}, MoErs1$^{\beta11}$ and MoErs1^{All}, while MoErs1^{L4} and MoErs1^{L8} have no inhibitory activities (Fig. 3b). Importantly, we found that the L2 and β11 regions have a more prominent role in the virulence of *M. oryzae*, in contrast to L4 and L8, which is consistent with their respective inhibitory activities (Fig. 3c–e). Notably, none of these mutants have defects in vegetative growth (Supplementary Table 2), indicating that the interaction sites between MoErs1 and OsRD21 are not the sites regulating vegetative growth.

To determine whether the inhibition of OsRD21 occurs during *M. oryzae* infection in a MoErs1-dependent manner, we further generated *OsRD21* gene knockout (*OsRD21*-KO) transgenic rice lines (Supplementary Fig. 12a). The *OsRD21*-OX plant was inoculated with Guy11, Δ*Moers1*, Δ*Moers1*-expressing *MoERS1* mutants with the native promoter, the complemented strain with the native promoter (Δ*Moers1*/*MoERS1*) and the constitutive rp27 promoter (Δ*Moers1*/*MoERS1*^{rp27}). After 48 hpi, leaves were harvested for total protein extraction and purification. The results showed that the Δ*Moers1*,

Fig. 3 | MoErs1 functions as a PLCP inhibitor to inhibit the activity of OsRD21. **a**, A structural model for the MoErs1–OsRD21 interaction predicted by ClusPro. Top: the surface of the MoErs1–OsRD21 complex. Middle: the interaction interface with amino acid residues shown as ribbon diagrams. Bottom: table showing three loops (L2, L4 and L8) and one β-strand (β11) with interaction sites of MoErs1. The sticks in different colours indicate corresponding interacting amino acids between MoErs1 and OsRD21. The yellow dotted line indicates hydrogen bonding and the orange dotted line indicates non-covalent binding. **b**, MoErs1 inhibits the PLCP activity of OsRD21. Top: model of the structure and processing of OsRD21. OsRD21 maturation comprising signal peptide release resulting in ProRD21, prodomain cleavage and final granulin domain removal to produce mature RD21 (mRD21). Bottom: GFP-tagged MoErs1 or the interaction site mutations in **a** were transiently expressed in *N. benthamiana* together with a FLAG fusion of OsRD21. Total proteins were extracted and purified, and labelled with 2 μM DCG-04 for 4 h. Proteins were separated by SDS–PAGE, detected with streptavidin-HRP, and chemiluminescence and immunoblotting with anti-FLAG and anti-GFP antibodies. The experiments were repeated independently at least 3 times with similar results. **c**–**e**, The interaction sites of MoErs1 contribute to virulence. Conidial suspensions (5×10^4 conidia per ml in 0.2% gelatin) of Guy11, the Δ*Moers1* mutant, the point mutation mutants and the complement strains were sprayed onto 2-week-old CO39. Diseased rice leaves were photographed after 7 dpi (**c**, top). The total protein of all the strains was extracted and detected with anti-GFP and anti-actin antibodies (**c**, bottom). DLA was assessed using Image J (**d**) and fungal growth was evaluated by quantifying *M. oryzae* genomic 28S rDNA relative to rice genomic Rubq1 DNA (**e**). Mean ± s.d. of 3 determinations. Significant differences were determined using two-sided Duncan's new multiple-range tests and marked with different letters.

https://doi.org/10.1038/s41477-024-01642-x

MoErs1^{L2} and MoErs1$^{\beta11}$ mutants could hardly inhibit the activity of OsRD21 because of their lower binding affinity, which is consistent with the previous interaction assay (Supplementary Fig. 10). Guy11, MoErs1^{L4}, MoErs1^{L8} and Δ*Moers1*/*MoERS1* all have moderate inhibitory activities. The Δ*Moers1*/*MoERS1*^{rp27} strain with high MoErs1 expression levels significantly inhibited the activity of OsRD21 (Supplementary Fig. 12b). These results are consistent in that inhibition of OsRD21 is MoErs1 dependent.

To assess the contribution of OsRD21-mediated host resistance against *M. oryzae*, the susceptible rice plant TP309, *OsRD21*-KO and *OsRD21*-OX were inoculated with Guy11, Δ*Moers1*, Δ*Moers1*-expressing *MoERS1* mutants, Δ*Moers1*/*MoERS1* or Δ*Moers1*/*MoERS1*^{rp27}. The results showed that *OsRD21*-OX lines have enhanced resistance against these strains, with fungal growth decreased by >60%. Growth was moderately compromised in plants inoculated with Δ*Moers1*/*MoERS1*^{rp27} strains (Supplementary Fig. 12c,d). Notably, the virulence of Δ*Moers1*,

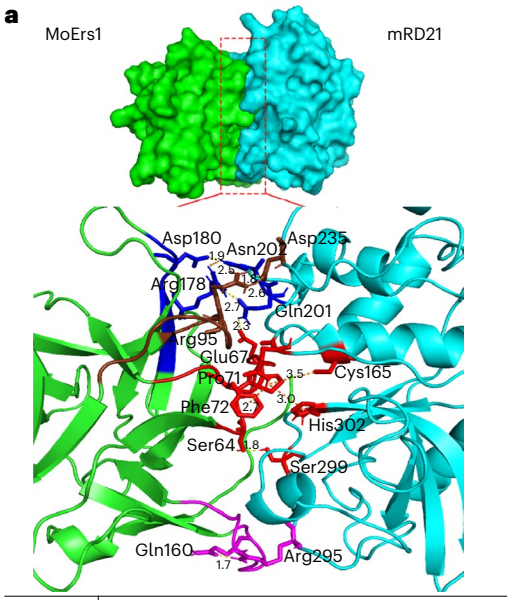

Regions	Predicted interaction sites of MoErs1
L2	S64, E67, P71, F72 (red)
L4	R95 (chocolate)
L8	Q160 (magenta)
β11	R178, D180 (blue)

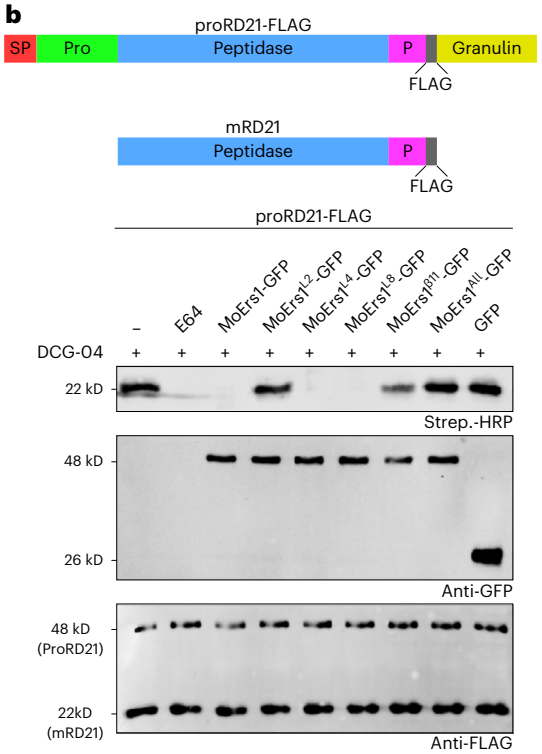

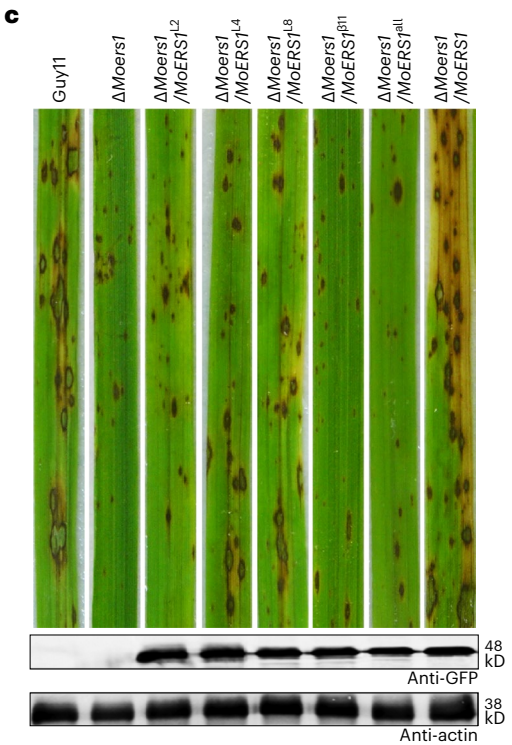

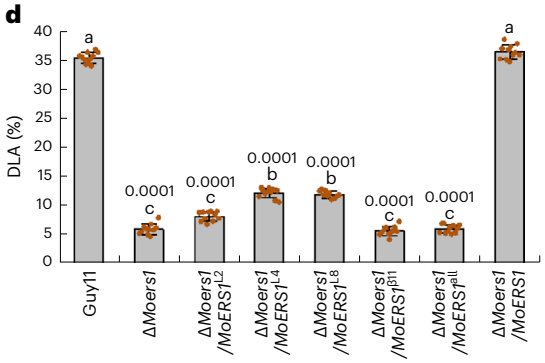

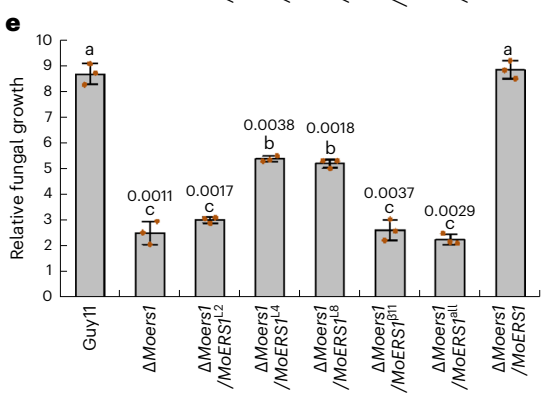

https://doi.org/10.1038/s41477-024-01642-x

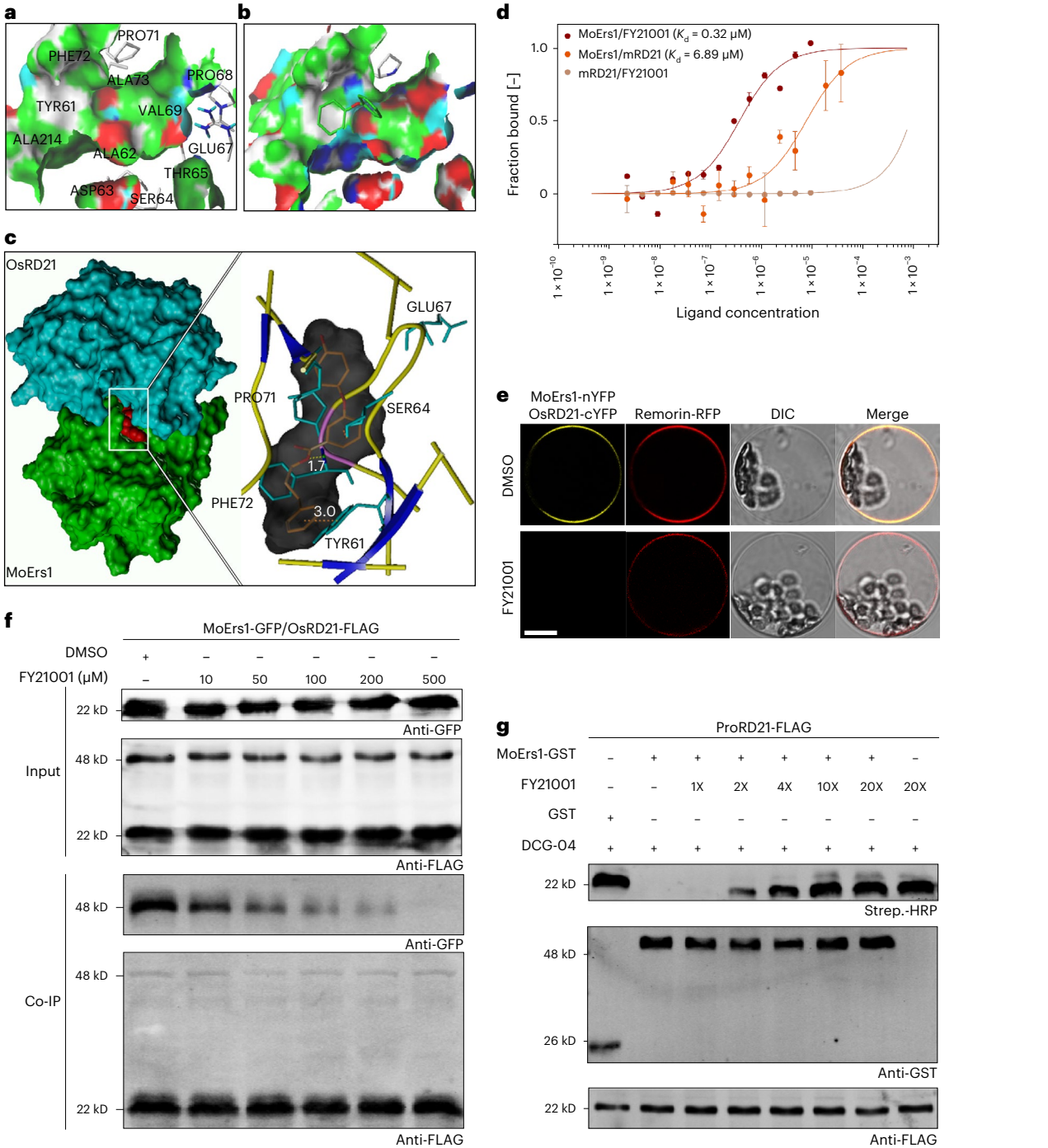

Fig. 4 | The diphenyl ether ester compound inhibits the inhibitory activity of MoErs1. a, The interaction region of MoErs1 and OsRD21. **b**, The molecular docking model of diaryl ether–MoErs1. **c**, The interaction model of MoErs1 (green)–OsRD21(blue), with the red area representing the compound FY21001. The key residues surrounding the active site are shown as green sticks. The yellow dotted line with the marked distance indicates hydrogen binding between FY21001 and amino acid residues Phe72 in MoErs1. The orange dotted line indicates non-covalent binding. **d**, FY21001 exhibits a stronger MoErs1 binding affinity than OsRD21, as assessed using MST. GST-MoErs1 (10 μM) was labelled with RED-NHS. The raw data were integrated and fitted to a binding model using the MST analysis software. The recombinant proteins were contained in NT standard capillaries. The solid curve is the fit of the datapoints to the standard K_d-fit function. Each binding assay was repeated independently three times ($n = 3$) and error bars represent s.d. **e**, BiFC assay showed that FY21001 inhibits the interaction between MoErs1 and OsRD21 in vivo. Co-expression of MoErs1-nYFP and OsRD211-cYFP, with PM marker Remorin-RFP, treated with DMSO or 500 μM FY21001 in rice protoplast cells, showed that fluorescence was detected when treated with DMSO, but not with FY21001. Scale bar, 10 μm. **f**, Co-IP assay showed that FY21001 inhibits the interaction between MoErs1 and OsRD21 in a dose-dependent manner in vivo. Co-expression of MoErs1-GFP and OsRD21-FLAG in rice protoplast cells treated with FY21001 in different concentrations. Immunoprecipitates obtained with the anti-FLAG antiserum and total protein extracts were immunoblotted with anti-FLAG and anti-GFP antibodies. **g**, GST-tagged MoErs1 was expressed and purified from *E. coli* strain BL21. FLAG-tagged OsRD21 was transiently expressed in *N. benthamiana*. Total proteins were extracted, purified and labelled with 2 μM DCG-04 for 4 h in the presence of compound FY21001 in a dose-dependent manner. Proteins were separated using SDS–PAGE and detected with streptavidin-HRP, and chemiluminescence and immunoblotting with anti-FLAG and anti-GST antibodies. All experiments were repeated independently at least 3 times with similar results.

MoErs1^{L2} and MoErs1$^{\beta11}$ was significantly rescued in *OsRD21*-KO when compared with TP309 (Supplementary Fig. 12c,d). Importantly, OsRD21 transgenic rice plants remained susceptible to *B. oryzae* and *X. oryzae* infection (Supplementary Fig. 12e,f), and OsRD21 expression was not responsive to *B. oryzae* and *X. oryzae* infection (Supplementary Fig. 12g,j). Moreover, OsRD21-mediated resistance was associated with the activation of the *PR1* gene (Supplementary Fig. 13). These results suggest that MoErs1 can function as a PLCP inhibitor to suppress OsRD21-mediated host immunity.

Diphenyl ether ester compounds inhibit MoErs1 function

To examine *MoERS1* conservation, we performed single-nucleotide polymorphism analysis on sequenced rice blast isolates from the NCBI database (Supplementary Table 4). In addition, a BLASTp search using the non-redundant protein sequences database with 500 target sequences failed to reveal any homologues of MoErs1 from other species, even in fungi (*E*-value < 10^{-30}) (Supplementary Fig. 14). This prompted us to explore whether MoErs1 could be a specific target for small-molecule compounds. According to the docking model, interaction sites between MoErs1 and OsRD21 are mainly within a long and narrow surface region, and there are more hydrophobic amino acid residues on the interface, which suggests that flexible molecules may facilitate the binding (Fig. 4a). Recently, diaryl ether was applied widely in agrochemical agents due to its sufficient molecular flexibility, excellent metabolic stability and pharmaceutical properties[43]. In addition, the diaryl ether scaffold contains two aromatic ring systems and a flexible oxygen bridge, leading to sufficient molecular flexibility and excellent lipid solubility, which can significantly increase cell membrane penetration. Considering these remarkable advantages, we selected diphenyl ether ester as a core skeleton unit of inhibitors. The Sybyl-x-2.0 molecular docking analysis of diaryl ether–MoErs1 revealed that oxygen atoms form hydrogen bonds with the N-H of Phe72. In addition, the two benzene rings are oriented towards the hydrophilic region (Ser64, Glu67) and the hydrophobic region (Phe72, Tyr61, Pro71), respectively (Fig. 4b). To enhance the binding stability between inhibitor molecules and targets, we introduced hydroxyl and ester groups to the diphenyl ether skeleton, facilitating hydrogen bonds and hydrophobic interactions.

Several derivatives were synthesized on the basis of the aforementioned skeleton and among them, FY21001 exhibited the lowest binding energy (−15.9 kcal mol^{-1}) and dissociation constant (K_d = 0.32 μM) with MoErs1 (Supplementary Tables 5 and 6). FY21001 was found to bind to the interaction area of MoErs1 and OsRD21. In the binding model of FY21001 with MoErs1, a hydrogen bond with Phe72 and a π−π hydrophobic interaction between phenylpropyl and Tyr61 were observed (Fig. 4c). To determine the specificity of FY21001 to MoErs1, we performed an MST assay that showed a stronger binding ability of FY21001 to MoErs1 than to OsRD21 (Fig. 4d), AtWSCP or OsWSCP (Supplementary Fig. 15a). When the rice protoplast expressing MoErs1-nYFP and OsRD21-cYFP was treated with 500 μM FY21001, the in vivo interaction was completely abolished (Fig. 4e). We then performed a co-IP assay in the rice protoplast and found that FY21001 reduces the binding affinity between MoErs1 and OsRD21 in a dose-dependent manner and that at 500 μM, FY21001 could completely abolish the interaction (Fig. 4f). These results suggest that FY21001 competes with OsRD21 in binding to MoErs1.

FY21001 inhibits the PLCP inhibitor activity of MoErs1 in a dose-dependent manner (Fig. 4g). In addition, alanine substitution mutations in L2 and β11 significantly reduced the interaction between FY21001 and MoErs1 (Supplementary Fig. 15b). We also found two derivatives, FY21003 and FY21019, with strong binding to MoErs1 (Supplementary Fig. 16a and Table 6). These two derivatives significantly inhibited the function of MoErs1 by relieving the inhibition of OsRD21 protease activities (Supplementary Fig. 16b). These results demonstrate that diphenyl ether ester compounds are effective in inhibiting the function of MoErs1 and have the potential to disrupt the MoErs1-dependent virulence of *M. oryzae*.

Diphenyl ether ester effectively controls rice blast

To examine whether these compounds can be explored as antifungal compounds to manage rice blast, we applied FY21001 at a concentration of 500 μM in infection under laboratory conditions. We found that FY21001 significantly reduced the lesion area and hyphal growth on rice leaves (Fig. 5a). Further comparative infection assays using these three compounds indicated that FY21001 has the best preventive half-maximum effective concentration (EC_{50}) at a concentration of 231.07 μM, which is similar to that of tricyclazole (EC_{50} = 224.08 μM) (Supplementary Table 7), a mainstream and high-efficiency fungicide for controlling rice blast. There were some slight reductions in EC_{50} with FY21003 (258.9 μM) and FY21019 (246.69 μM) (Supplementary Tables 6 and 7). To further test their applications, we carried out a preventive effect test using three different settings: (1) co-treatment with *M. oryzae* spores, (2) pre-treatment for 24 h and (3) post-treatment for 24 h. The results showed that co-treatment and pre-treatment have the best controlling effect, followed by post-treatment (Fig. 5a–d). FY21001 also showed an effective preventive effect against the neck

Fig. 5 | Diphenyl ether ester compounds are effective against rice blast. **a**,**b**, FY21001 is effective against rice leaf blast. Rice leaves were sprayed with 500 μM of compounds with either 24 h co-inoculation, pre-inoculation or post-inoculation with Guy11 spores. Diseased rice leaves were photographed after 7 dpi (**a**). The biologically independent DLA (**b**, top) is displayed as boxes with individual datapoints (n = 21). The error bars represent maximum and minimum values. Centre line, median; box limits, 25th and 75th percentiles. Fungal growth (**b**, bottom) was measured by quantifying *M. oryzae* genomic 28S rDNA relative to rice genomic Rubq1 DNA. Mean ± s.d. of 3 determinations. Significant differences were determined by two-sided Duncan's new multiple-range tests and marked with different letters. **c**,**d**, Conidiation lesions on surface-sterilized rice leaves in **a** were counted and photographed (**c**). The lesions producing conidia (typical lesions) and those that fail to produce conidia (necrotic lesions) are quantified (**d**). Error bars represent s.d. **e**,**f**, FY21001 is effective against rice neck blast in the field. **e**, Neck blast severity was evaluated using the standard 0–9 scale, rated on six levels defined as follows: level 0: no visible lesion or observed lesions on only a few pedicels; level 1: lesions on several pedicels or secondary branches; level 3: lesions on a few primary branches or the middle part of the panicle axis; level 5: lesion partially around the base (node) or the uppermost internode or the lower part of panicle axis near the base; level 7: lesion completely around panicle base or uppermost internode or panicle axis near the base with more than 30% of filled grains; level 9: lesion completely around panicle base or uppermost internode or the panicle axis near the base with less than 30% of filled grains (International Rice Research Institute Standard Evaluation System for Rice). **f**, Field resistance to neck blast was assessed in a natural rice blast nursery (Jiangsu Province, China). Three plots were established in the field. One thousand susceptible rice plants were planted in each plot. One group treated with 500 μM DMSO was used as the negative control, one group treated with 500 μM tricyclazole (TCZ) was used as the positive control and the trial group was treated with 500 μM FY21001. **g**, Statistics of disease index. Disease index = 100 × Σ (number of diseased leaves at all levels × representative value at all levels)/(total leaves investigated × highest representative value) (n = 3 biologically independent samples). **h**, Grain yield of Nip treated with FY21001, tricyclazole or DMSO under natural blast nursery conditions. Significant differences were determined using Duncan's new multiple-range tests and marked with different letters (n = 3 biologically independent samples). **i**, Wild-type TP309 and OsRD21-KO transgenic rice leaves sprayed with or without FY21001 (500 μM) for 24 h were inoculated with Guy11 and the Δ*Moers1* mutant (1×10^5 spores per ml). **j**, The biologically independent DLA is displayed as boxes with individual datapoints (n = 10). The error bars represent maximum and minimum values. Centre line, median; box limits, 25th and 75th percentiles. **k**, Fungal growth measured by quantifying *M. oryzae* genomic 28S rDNA relative to rice genomic Rubq1 DNA. Mean ± s.d. of 3 determinations. Significant differences were determined using two-sided Duncan's new multiple-range tests and marked with different letters.

https://doi.org/10.1038/s41477-024-01642-x

blast in a natural rice blast nursery, similar to tricyclazole (Fig. 5e–g), and the efficacy was higher compared with cafenstrole and metazachlor (Supplementary Fig. 17)[44]. Moreover, FY21001 and tricyclazole-treated Nip (Nipponbare) rice reduced grain yield losses by over 60% compared with dimethylsulfoxide (DMSO)-treated Nip control rice in the blast nursery (Fig. 5h). There were six rice blast isolates (Jiangsu #1–6) separated from the nursery; all of them contain the *MoERS1* gene and are without sequence polymorphism (Supplementary Table 4).

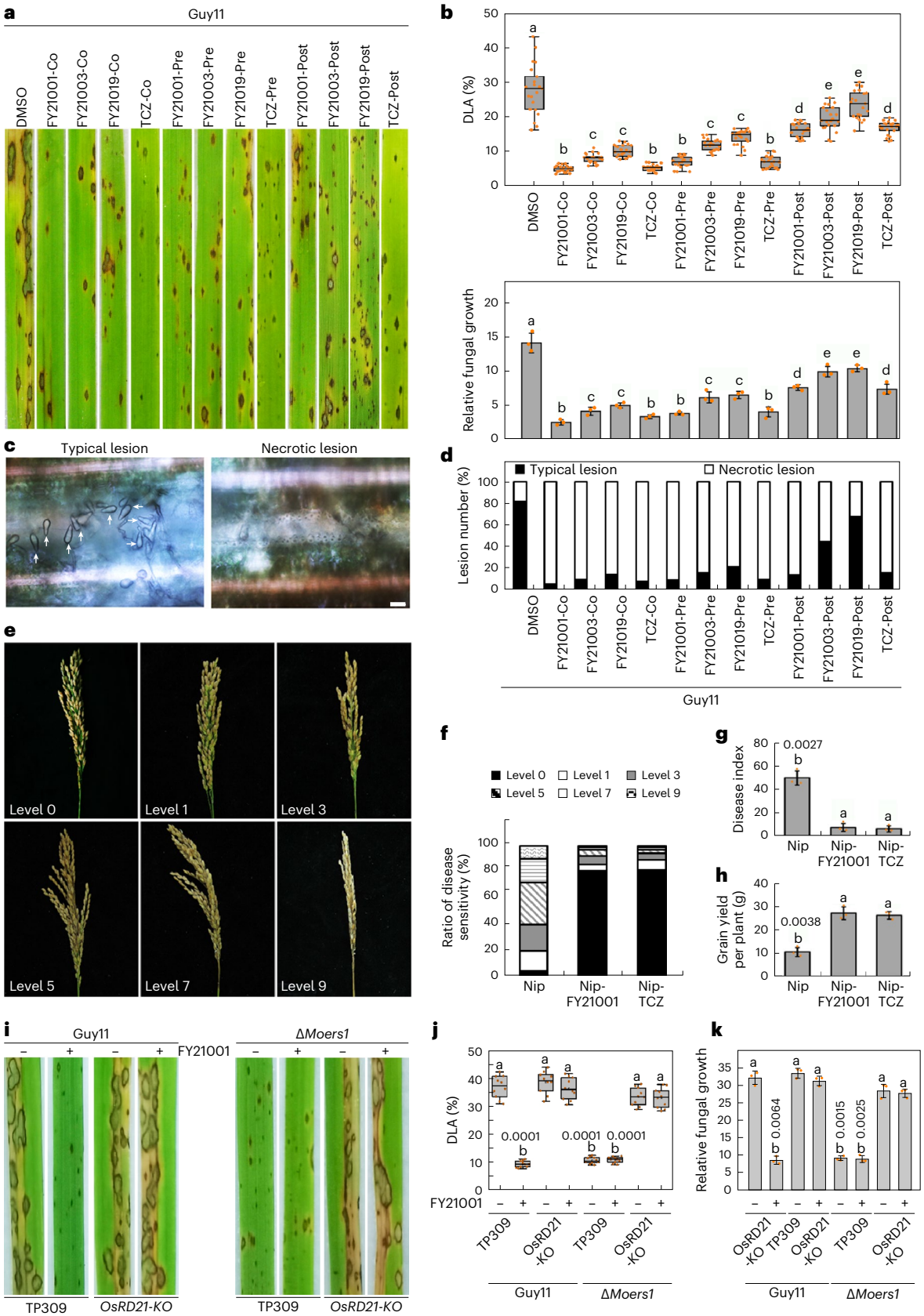

https://doi.org/10.1038/s41477-024-01642-x

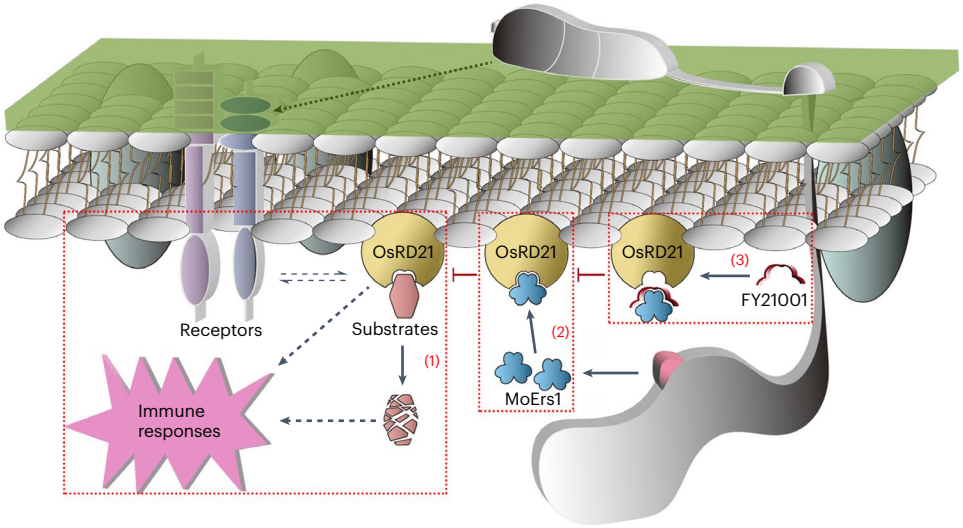

Fig. 6 | A proposed model of MoErs1 function to suppress host immunity. There are 3 states of OsRD21 during the *M. oryzae*–rice interaction when treated with compound FY21001. (1) Rice cells perceive the infection via the functions of transmembrane receptors and, at the same time, PLCP OsRD21-mediated substrate degradation allows the activation of the host immune response. (2) *M. oryzae* secretes the effector protein MoErs1 during its interaction with the rice host. MoErs1 targets OsRD21 and suppresses its PLCP activities. (3) FY21001, a diphenyl ether ester, specifically binds MoErs1 to inhibit its function, which relieves the inhibition of OsRD21 protease activities to promote host immunity against *M. oryzae* infection.

To substantiate whether FY21001 suppresses disease via interfering with MoErs1 function, we performed an infection assay of TP309 and *OsRD21*-KO transgenic rice plants with Guy11 and the Δ*Moers1* mutant with or without FY21001 treatment. The results revealed that FY21001 treatment effectively inhibited the infection of Guy11 on TP309 but had no effect on the infection of Guy11 on *OsRD21*-KO rice plants. Notably, the reduced virulence of Δ*Moers1* on TP309 was restored when tested on *OsRD21*-KO rice plants, irrespective of the presence or absence of FY21001 treatment (Fig. 5i–k). These findings suggest that the disease-suppressing effect of FY21001 depends on the presence of MoErs1 and OsRD21.

Notably, FY21001 neither conferred any resistance against *B. oryzae* and *X. oryzae* lacking the *MoERS1* gene (Supplementary Fig. 18), nor affected the development of *M. oryzae* (Supplementary Fig. 19). The DAB staining assay showed that the application of these compounds results in a reduced ability of *M. oryzae* to scavenge host ROS (Supplementary Fig. 20a). We carried out further infection assays on rice sheaths and found that FY21001 treatment can significantly inhibit invasive hyphae growth, an effect similar to that exhibited by the Δ*Moers1* mutant. Notably, the infectious defect was rescued in the presence of diphenyleneiodonium (Supplementary Fig. 20b), indicating that FY21001 inhibits invasive hyphae growth via disruption of the MoErs1–OsRD21 interface. This effect is similar to that exhibited by the Δ*Moers1* mutant.

Finally, to investigate whether FY21001 induces rice immunity, we examined the transcriptional levels of different disease-resistance genes in the host, including *PR1*, *PBZ1*, *AOS2*, *LOX1* and NADPH oxidases *RBOHA* and *RBOHB*. None of these genes showed any changes in expression in the presence of FY21001 (Supplementary Fig. 21a,b). To further determine whether FY21001 induces ROS burst in planta, TP309, *OsRD21*-KO and *OsRD21*-OX rice leaf discs were treated with FY21001, FLG22 (a bacterial flagella peptide that elicits strong plant defence) or DMSO. Interestingly, FLG22 induced a higher ROS accumulation in the *OsRD21*-OX rice line than in TP309 and *OsRD21*-KO. However, ROS levels were not affected in the presence of FY21001 or DMSO (Supplementary Fig. 21c), indicating that FY21001 cannot induce rice immune responses. These results suggest that FY21001 and its derivatives have a preventive protection role against *M. oryzae* infection.

Discussion

Plant pathogens secrete effector proteins that are important for successfully colonizing host plants. Previous studies have also demonstrated that these effectors target various host components to interfere with host immunity. At the same time, plants utilize mechanisms such as PLCPs in their immune responses, targeting these pathogens and their effectors[12–14]. As demonstrated, the overexpression of OsRD21 in rice confers enhanced resistance against *M. oryzae*.

Previous studies also indicated that most PLCPs function in apoplasts[12,18,21,22]. However, some also function in other cellular compartments. For example, RD19 is localized to the mobile vacuole-associated compartments[17], XCP2 interacts with PRN2 in the cytosolic compartments[45] and CYP1 is co-localized with the tomato yellow leaf curl virus (TYLCV) V2 protein in the cytoplasm[16]. RD21 proteins appear to have multiple subcellular locations. It has been reported that AtRD21 accumulates in the vacuoles, ER bodies[36], the PM and apoplastic spaces[11]. Notably, two different protease inhibitors, the serine protease inhibitor AtSerpin1[36,46] and the Kunitz protease inhibitor AtWSCP[34,47,48], were found to inhibit RD21 in the cytoplasm but not in the apoplast. These findings are consistent with the fact that RD21 functions in intracellular components rather than extracellular spaces. Our data showed that OsRD21 is not secreted into the apoplast but is mainly localized in the PM of the host.

Moreover, previous studies have shown that PLCPs are the common targets of a variety of pathogen-secreted effectors[11,12,16–22]. We have demonstrated that *M. oryzae* MoErs1 physically interacts with RD21 on the PM and functions as a PLCP inhibitor to regulate OsRD21 activities. Owing to the structural similarity with host WSCPs, a strong possibility is that MoErs1 might mimic PLCPs to suppress the activity of RD21 in vivo, which represents a new inhibition mechanism.

Despite the importance of fungal effectors in pathogenicity, it remains unknown whether these effectors can be utilized as novel fungicides to inhibit rice blast. In addition, most recent investigations were based on existing chemicals to identify the targets, which yielded limited progress. We set out to design chemicals with sound control effects against the blast pathogen based on pathogenic mechanisms. During the co-evolution of pathogens and hosts, it is thought that the effectors are often unstable and change due to mutations allowing the evasion of host recognition[49–51]. This would result in any effector-based

fungicidal development not being effective in the long term. However, there are still some evolutionarily conserved effectors playing important roles in pathogenicity, such as HaRxL23, PsAvh73 and PRS2 of oomycetes and Fol-SIX4 of *Fusarium oxysporum*[52–54]. We found that MoErs1 is evolutionarily conserved and has no homologues in other species, making it an ideal target for novel fungicide evaluation. On the basis of the MoErs1–OsRD21 docking model, we designed the diphenyl ether ester compound FY21001 that inhibits MoErs1 function (Fig. 6). Importantly, we showed that the application of FY21001 effectively controls blast in the rice field, suggesting a strong potential of FY21001 as a new class of fungicide. Since MoErs1 is specific to *M. oryzae*, the effectiveness of FY21001 in managing other diseases of rice is limited.

Our study provided presumably the first example of how compounds targeting species-specific effector proteins of fungal origins could be employed as a novel fungicide. Since most effectors are fungal specific and absent in plants, the development of such compounds targeting these effectors would provide an environmentally safe and ecologically sustainable way of managing crop diseases.

Methods

Fungal strains and cultures

M. oryzae Guy11 was used as the wild-type strain in this study. The knockout mutant Δ*Mosyn8* was characterized previously by us[23]. All strains were cultured in CM medium. Liquid CM was used to prepare mycelia for DNA and RNA extraction. For conidiation, strain blocks were maintained on a straw decoction and corn agar medium at 28 °C for 7 days in the dark, followed by 3 days of continuous illumination under fluorescent light.

Secreted protein extraction

Secreted proteins were prepared as previously described[24]. Briefly, fungal strains were cultured in MMN medium for 2 days at 28 °C and collected. The cultures were extracted with 0.5 times the volume of phenol by shaking on ice for 15 min, followed by centrifugation at 1,500 *g* for 20 min. This phenol extraction was repeated twice. The phenol layer was then precipitated by adding 4 volumes of 100 mM ammonium acetate in methanol at −20 °C for 5 h. Precipitated proteins were recovered by centrifugation at 1,500 *g* for 15 min. The pellet was washed twice with 80% methanol containing 100 mM ammonium acetate, and then once with 80% acetone before storage at −20 °C.

2D-E and quantitative analysis

For 2D-E, the secreted protein crude extracts were vacuum dried and then dissolved in 800 µl lysis solution containing 7 M urea, 2 M thiourea, 4% (w/v) 3-[(3-cholamidopropyl)-dimethylammonium]-1-propanesulfonate, 65 mM dithiothreitol (DTT), 1 mM PMSF and 0.5% (v/v) biolytes (Bio-Rad). Insoluble materials were removed by centrifugation and proteins were quantified using the Bradford method. About 1,200 µg protein was separated by loading on an 18-cm pH 4–7 nonlinear gradient IPG strip (GE Healthcare). The second electrophoretic dimensional separation was carried out on a 12% SDS–PAGE. Signals were observed using Coomassie brilliant blue (CBB) G-250. The gel image was digitalized with a gel scanner (Powerlook 2100XL, UMAX) and analysed with the PDQuest software package (v.7.2.0; Bio-Rad). Spots were detected, matched and normalized on the basis of the total density of gels with the parameter of percent volume according to the software guide. For each spot, the mean relative volume was computed, and spots showing a mean relative volume that changed more than 1.5-fold and $P < 0.05$ in different stages were considered differentially expressed proteins.

Matrix-assisted laser desorption/ionization–time of flight (MALDI–TOF) analysis

For in-gel digestion and MALDI–TOF analysis, protein spots with differential expression patterns were manually excised from gels, washed with Millipore pure water three times and destained twice with 50 mM NH_4HCO_3 in 50% acetonitrile for CBB G-250 staining spots. Samples were then processed as follows: reduction with 10 mM DTT in 50 mM NH_4HCO_3, alkylation with 40 mM iodoacetamide in 50 mM NH_4HCO_3, drying twice with 100% acetonitrile and digestion overnight at 37 °C with sequencing-grade modified trypsin (Promega) in 50 mM NH_4HCO_3. The peptides were extracted twice with 0.1% trifluoroacetic acid in 50% acetonitrile. Extracts were pooled and lyophilised. The resulting lyophilised tryptic peptides were dissolved in 5 mg ml^{-1} α-Cyano-4-hydroxycinnamic acid containing 0.1% trifluoroacetic acid and 50% acetonitrile. MALDI–TOF/TOF MS analyses were conducted using a Bruker Daltonics Ultraflex MALDI–TOF/TOF analyser. All spectra of proteins were submitted for database search using the online MASCOT programme (http://www.matrixscience.com) against NCBInr databases. The search parameters were as follows: 0.15 Da mass tolerance for peptides and 0.25 Da mass tolerance of TOF/TOF fragments, one allowed trypsin miscleavage, carbamidomethyl of Cys as fixed modification, and oxidation of Met, pyro-Glu formation of N-terminal Gln and Glu as variable modification. Only significant hits, as defined by the MASCOT probability analysis ($P < 0.05$), were accepted.

Construction of *MoERS1* vectors

To analyse the function of MoErs1, we created the targeted gene deletion vector pMD-*MoERS1-HPH* by inserting the *HPH* gene cassette between the two flanking sequences of the *MoERS1* gene. A 1 kb upstream flanking sequence and 1 kb downstream flanking sequence were amplified from *M. oryzae* genomic DNA by PCR using primer pairs *MoERS1*-p1 (F)/*MoERS1*-p2 (R) and *MoERS1*-p3 (F)/*MoERS1*-p4 (R), respectively. The two flanking sequences were linked by overlap PCR with primer pairs *MoERS1*-p1 (F)/*MoERS1*-p4 (R), and the amplified 2 kb fragments were purified and cloned into a pMD19-T vector (Takara) to generate the plasmid pMD-*MoERS1*. An EcoRV restriction site was incorporated into primers *MoERS1*-p2/*MoERS1*-p3. The *HPH* gene cassette was prepared by PCR from the plasmid pCB1003 with primer pairs FL1111/FL1112 and inserted into the EcoRV site of pMD-*MoERS1* to generate the final disruption construct pMD-*MoERS1-HPH*. The 3.4-kb fragment was amplified with *MoERS1*-p1 (F)/*MoERS1*-p4 (R) primers and transformed into Guy11.

The transformants were screened using primers *MoERS1*-p5 (F)/*MoERS1*-p6 (R). For Southern blotting, the *MoERS1* gene probe was amplified using the primers *MoERS1*-p5 (F)/*MoERS1*-p6 (R), and the *HPH* gene probe was amplified using the primers FL1111/ FL1112. For complementation, a fragment containing the *MoERS1* gene and its native promoter regions was amplified by PCR with primers *MoERS1*-p7 (F)/*MoERS1*-p8 (R) and inserted into the pYF11 (bleomycin resistance) vector, generating pYF11-*MoERS1*-GFP. The construct was used for the protoplast transformation of the Δ*Moers1* mutant. The resulting transformants were screened by phenotype characterization, including growth restoration, and verified by PCR amplification.

Infection assays

For the virulence test, conidia were suspended to a concentration of 5×10^4 spores per ml in a 0.2% (w/v) gelatin solution, and 4 ml each was sprayed on 2-week-old rice seedlings (*Oryza sativa* CO39). Inoculated plants were kept in a growth chamber at 25 °C with 90% humidity and in the dark for the first 24 h, followed by a 16/8 h light/dark cycle. Disease severity was assessed at 7 days after inoculation. Fungal growth was determined using qPCR to measure the amount of *M. oryzae* genomic 28S ribosomal DNA (rDNA) relative to rice genomic Rubq1 DNA. PCR primers are listed in Supplementary Table 8. For observation of the penetration and invasive growth in rice cells, conidial suspensions (1×10^5 spores per ml) were injected into the leaf sheath. At 28 °C for 24 or 48 h, the inner epidermis of infected sheaths was observed under a microscope. Experiments were repeated three times.

Confocal microscopy was performed using a ZEISS LSM710 microscope. Excitation/emission wavelengths were 488/505 nm for eGFP and 543/560 nm for RFP, respectively. Images were acquired and processed using LSM710 ZEN software (Zeiss).

ROS assessment

To observe ROS derived from the host, rice leaves or sheaths were stained with DAB (Sigma-Aldrich) as previously described[55]. To measure ROS levels, leaves were cut into discs with a cork borer and pre-incubated overnight in sterile-distilled water. After the leaf discs were treated with DMSO, FLG22 or other agents, ROS production was monitored using the luminol chemiluminescence assay[29]. This experiment was repeated three times.

RNA isolation and RT–qPCR

For quantification of gene expression, RNA was isolated using TRIzol reagent (Invitrogen). Complementary (c)DNA synthesis was performed using PrimeScript RT reagent kit (Takara). RT–qPCR was performed with the ABI 7500 fast real-time system and transcripts were analysed using the 7500 System SDS software. To compare the relative abundance of *PR* gene transcripts, the average threshold cycle (C_t) was normalized to rice actin for each of the treated samples as $2^{-\Delta C_t}$, where $-\Delta C_t = (C_t \text{ target gene} - C_t \text{ actin})$. Fold changes were calculated as $2^{-\Delta\Delta C_t}$, where $-\Delta\Delta C_t = (C_t \text{ experiment} - C_t \text{ actin}) - (C_t \text{ control} - C_t \text{ actin})$. All experiments were repeated three times. Primers used are listed in Supplementary Table 8.

Generation and characterization of transgenic rice

Oryza sativa japonica cv. TP309 was transformed with the constructs pCam2300-Pro_{actin1}:*OsRD21-FLAG*, pCam2300-Pro_{actin1}:*MoERS1-FLAG* and CRISPR-Cas9:*OsRD21*, with *Agrobacterium tumefaciens*-mediated transformation at Edgene Bio. The overexpression lines were characterized by western blotting and knockout lines were characterized by DNA sequencing.

Y2H assay

For the Y2H assay, the *MoERS1* or *PLCPs* cDNA sequence was amplified and cloned into pGBKT7 or pGADT7, respectively. Yeast transformation and screening were performed according to manufacturer instructions (Clontech). Yeast AH109 cells were co-transformed with specific bait and prey constructs. All yeast transformants were grown on an SD/-Leu/-Trp/-His/-Ade medium for selection.

co-IP

Co-IP of *N. benthamiana* cells was performed as previously described[56]. Briefly, samples were extracted with the IP buffer (50 mM Tris-HCl pH 7.5, 150 mM NaCl, 0.5% NP-40, 5 mM DTT and protease inhibitor cocktail). The mixtures were kept at 4 °C with gentle shaking for 1 h. The IP complex was captured by adding 50 µl GFP-Trap (ChromoTek) or anti-FLAG M2 affinity gel (Sigma), followed by shaking at 4 °C for another 1 h. The beads were recovered by centrifugation at 2,500 × *g* for 30 s and washing six times with cold TBS buffer (50 mM Tris-HCl pH 7.5, 150 mM NaCl). Then 50 µl of glycine eluting solution (pH 2.5) was added to the beads. After boiling for 5 min, the samples were loaded onto the SDS–PAGE gels for western blot analysis, followed by detection with the anti-FLAG antibody (Engibody, 1:3,000 dilution) and anti-GFP antibody (Abmart, 1:5,000).

MST analysis

Binding reactions of recombinant GST-MoErs1 and its interaction site mutation proteins with OsRD21 or test compounds were measured by MST in a Monolith NT.Label Free (Nano Temper Technologies) instrument. Labelled GST-MoErs1 (10 µM) was displaced by a buffer. A range of concentrations of OsRD21 or test compounds in the assay buffer were incubated with labelled protein (1:1, v/v) for 10 min. The samples were loaded into the NT.Label Free standard capillaries and measured with 20% light-emitting diode power and 40% MST power. The K_d-fit function of the Nano Temper analysis software (v.1.5.41) was used to fit the curve and calculate the value of the K_d. Experiments were repeated three times.

Protein crystallization

Construction of expression vectors. The MoErs1 (21–214 amino acids (aa)) coding sequence was amplified from the cDNA library of *M. oryzae* strain Guy11 and cloned into the modified pET15b vector (Novagen). Site-directed mutagenesis of *MoErs1*$^{E112M/E191M}$ was carried out using the overlap PCR method. All plasmids were verified by DNA sequencing before protein expression and purification.

Protein expression and purification. MoErs1 (21–214 aa) containing N-terminal 6xHis tag, MysB protein and a cleavage site for the tobacco etch virus (TEV) protease was overexpressed in *E. coli* BL21 (DE3). *E. coli* cells were grown in liquid LB medium at 37 °C to an optical density $(OD)_{600}$ of 0.4–0.8. The temperature of the culture was then lowered to 16 °C and the expression of MoErs1 was induced by the addition of 0.4 mM isopropyl β-D-1- thiogalactopyranoside. After 12 h, cells were collected by centrifugation at 5,300 *g* for 15 min. The cell pellet was resuspended in lysis buffer (20 mM Tris-HCl pH 8.0, 200 mM NaCl, 10 mM imidazole) supplemented with 1 mM PMSF, lysed with a high-pressure homogenizer and then centrifuged at 37,000 *g* for 50 min at 4 °C. The supernatant was loaded to a Nickel affinity column (GE Healthcare). Ten bed volumes of wash buffer (20 mM Tris-HCl pH 8.0, 200 mM NaCl, 30 mM imidazole) were used to wash the resin, and 3 bed volumes of elution buffer (20 mM Tris-HCl pH 8.0, 200 mM NaCl, 200 mM imidazole) were used to elute the target protein. The purity of the target protein was analysed by SDS–PAGE. The affinity-enriched proteins were further purified using an anion exchange column (GE Healthcare) and the tag was cleaved overnight at 4 °C with a molar ratio 1:20 TEV protease. Subsequently, the protein was purified using a Nickel affinity column and gel filtration chromatography (GE Healthcare). The protein peak was collected and then concentrated to 10 mg ml^{-1} (20 mM Tris-HCl pH 8.0, 800 mM NaCl, 5 mM DTT). All purification processes were performed at 4 °C.

Protein crystallization. The MoErs1 crystal structure was initially screened using the sitting drop method at 4 °C. After mixing 0.4 µl MoErs1 protein (10 mg ml^{-1} in 20 mM Tris-HCl pH 8.0, 800 mM NaCl, 5 mM DTT) with 0.4 µl reservoir solution, the screening plates were placed at 4 °C for crystal growth, which took 3 days. The hanging drop method was then used to further optimize the growth. MoErs1 (1.5 µl, 10 mg ml^{-1} in 20 mM Tris-HCl pH 8.0, 800 mM NaCl, 5 mM DTT) was mixed with an equal volume (1.5 µl) of the reservoir solution consisting of 0.05 M zinc acetate dihydrate and 20% polyethylene glycol 3350. Before data collection, all crystals were cryo-protected by gradient transfer into the reservoir solution containing 25% glycerol and flash frozen in liquid nitrogen.

Data collection and structure determination. The diffraction data of native MoErs1 (2.5 Å) and Se-Met MoErs1$^{E112M/E191M}$ (2.2 Å) crystals were collected at BL18U1 and BL17U1 beamline at the Shanghai Synchrotron Radiation Facility. The diffraction images were processed and scaled using HKL2000/3000 package (HKL Research). Phases were initially obtained for Se-Met MoErs1$^{E112M/E191M}$ data (21–214 aa). The structure of MoErs1 was solved using the single-wavelength anomalous diffraction method[31] as executed in Phenix[57]. The structural models were obtained using autosol and autobuild in Phenix and manually rebuilt with COOT[58], and Phenix was used to refine the structure further. All structure-related pictures in this research were produced using Pymol v.2.1.0 (Schrödinger).

Syntheses of target compounds

All solvents used were either chemically pure or analytically pure grade. The purity of commercially available reaction materials was maintained above 95%. The whole synthetic scheme for target compound FY21001 is shown below.

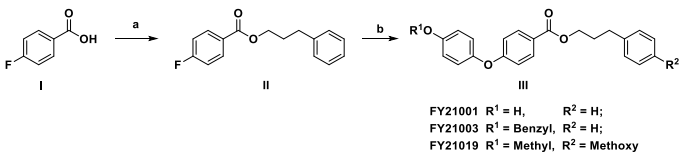

Synthetic route of the title compound. Reagents and conditions: **a**, $(COCl)_2$, dimethylformamide (DMF), substituted 3-phenylpropan-1-ol, dichloromethane (DCM), 0 °C; **b**, substituted phenol, K_2CO_3, DMF, 100 °C.

Synthesis of 3-phenylpropyl 4-fluorobenzoate (II). 4-fluorobenzoic acid (I, 2.0 mmol) was dissolved in the anhydrous DCM. $(COCl)_2$ (2.5 mmol) was slowly added dropwise to the reaction system at 0 °C. After stirring for 4 h, the reaction solution was removed under vacuum distillation. DCM was used to dissolve the remaining solids, and phenylpropanol (2.5 mmol) and trimethylamine (2.5 mmol) were then added. After 2 h, a $NaHCO_3$ solution (30 ml) was added to the reaction mixture with stirring and the organic phase was separated. The organic phases were combined, dried with Na_2SO_4 and purified by column chromatography to give the intermediate II 3-phenylpropyl 4-fluorobenzoate. Yield = 80%, ^{1}H NMR (500 MHz, DMSO-d_6) δ 8.01 (dd, J = 9.0, 5.5 Hz, 2H), 7.39–7.33 (m, 2H), 7.32–7.27 (m, 2H), 7.26–7.23 (m, 2H), 7.22–7.17 (m, 1H), 4.26 (*t*, J = 6.4 Hz, 2H), 2.77–2.71 (m, 2H), 2.07–1.99 (m, 2H). s indicates singlet, d indicates doublet, dd indicates doublet of doublets, *t* indicates triplet, m indicates multiplet, H indicates hydrogen atom, J indicates coupling constant, δ indicates chemical shift, the numbers indicate a range of peaks or signals.

Synthesis of 3-phenylpropyl 4-(4-hydroxyphenoxy) benzoate (FY21001). In an N_2 atmosphere, intermediate II (2.0 mmol), hydroquinone (4.0 mmol), K_2CO_3 (4.0 mmol) and DMF (10 ml) were added together into a 100-ml two-necked bottle. The mixture was stirred at 80 °C for 6 h. When the reaction was complete, 50 ml H_2O was added into the reaction system. The aqueous layer was extracted with ethyl acetate (20 ml) twice and the organic layers were combined, followed by drying with Na_2SO_4 and column chromatography purification to give the title compound FY21001. Yield = 50%, high-resolution mass spectrum: m/z [M + H]+ calculated for [C22H21O4]: 349.1439, Found: 349.1433. ^{1}H NMR (500 MHz, chloroform-d) δ 7.97 (d, J = 8.5 Hz, 2H), 7.31–7.26 (m, 2H), 7.23–7.18 (m, 3H), 6.97–6.90 (m, 4H), 6.86 (d, J = 9.0 Hz, 2H), 4.32 (*t*, J = 6.5 Hz, 2H), 2.80–2.74 (m, 2H), 2.09 (m, 2H). Other derivatives were similarly synthesized. s indicates singlet, d indicates doublet, dd indicates doublet of doublets, *t* indicates triplet, m indicates multiplet, H indicates hydrogen atom, J indicates coupling constant, δ indicates chemical shift, the numbers indicate a range of peaks or signals.

Reporting summary

Further information on research design is available in the Nature Portfolio Reporting Summary linked to this article.

Data availability

All data generated or analysed during this study are included in this published article and its supplementary files. Bio-reagents are available for research purposes upon request from the corresponding author under a Material Transfer Agreement. The NCBI non-redundant protein sequences (nr) database is available at https://blast.ncbi.nlm.nih.gov/Blast.cgi. The CDS sequence for the *MoRES1* gene is available in the NCBI database (accession no. OK562582).

References

1. Wang, X., Song, K., Li, L. & Chen, L. Structure-based drug design strategies and challenges. *Curr. Top. Med. Chem.* **18**, 998–1006 (2018).
2. Dodds, P. N. & Rathjen, J. P. Plant immunity: towards an integrated view of plant–pathogen interactions. *Nat. Rev. Genet.* **11**, 539–548 (2010).
3. Jones, J. D. & Dangl, J. L. The plant immune system. *Nature* **444**, 323–329 (2006).
4. Dong, S. M. & Ma, W. B. How to win a tug-of-war: the adaptive evolution of *Phytophthora* effectors. *Curr. Opin. Plant Biol.* **62**, 102027 (2021).
5. Zhang, H., Zheng, X. & Zhang, Z. The *Magnaporthe grisea* species complex and plant pathogenesis. *Mol. Plant Pathol.* **17**, 796–804 (2016).
6. Dean, R. et al. The top 10 fungal pathogens in molecular plant pathology. *Mol. Plant Pathol.* **13**, 414–430 (2012).
7. Khush, G. S. What it will take to feed 5.0 billion rice consumers in 2030. *Plant Mol. Biol.* **59**, 1–6 (2005).
8. D'Avila, L. S., De Filippi, M. C. C. & Cafe-Filho, A. C. Sensitivity of *Pyricularia oryzae* populations to fungicides over a 26-year time frame in *Brazil*. *Plant Dis.* **105**, 1771–1780 (2021).
9. Harata, K., Daimon, H. & Okuno, T. Trade-off relation between fungicide sensitivity and melanin biosynthesis in plant pathogenic fungi. *Iscience* **23**, 101660 (2020).
10. Skamnioti, P. & Gurr, S. J. Against the grain: safeguarding rice from rice blast disease. *Trends Biotechnol.* **27**, 141–150 (2009).
11. Bozkurt, T. O. et al. *Phytophthora infestans* effector AVRblb2 prevents secretion of a plant immune protease at the haustorial interface. *Proc. Natl Acad. Sci. USA* **108**, 20832–20837 (2011).
12. Kaschani, F. et al. An effector-targeted protease contributes to defense against *Phytophthora infestans* and is under diversifying selection in natural hosts. *Plant Physiol.* **154**, 1794–1804 (2010).
13. Paulus, J. K. et al. Extracellular proteolytic cascade in tomato activates immune protease Rcr3. *Proc. Natl Acad. Sci. USA* **117**, 17409–17417 (2020).
14. Shindo, T., Misas-Villamil, J. C., Horger, A. C., Song, J. & van der Hoorn, R. A. A role in immunity for *Arabidopsis* cysteine protease RD21, the ortholog of the tomato immune protease C14. *PLoS ONE* **7**, e29317 (2012).
15. Misas-Villamil, J. C., van der Hoorn, R. A. & Doehlemann, G. Papain-like cysteine proteases as hubs in plant immunity. *New Phytol.* **212**, 902–907 (2016).
16. Bar-Ziv, A., Levy, Y., Citovsky, V. & Gafni, Y. The tomato yellow leaf curl virus (TYLCV) V2 protein inhibits enzymatic activity of the host papain-like cysteine protease CYP1. *Biochem. Biophys. Res. Commun.* **460**, 525–529 (2015).
17. Bernoux, M. et al. RD19, an *Arabidopsis* cysteine protease required for RRS1-R-mediated resistance, is relocalized to the nucleus by the *Ralstonia solanacearum* PopP2 effector. *Plant Cell* **20**, 2252–2264 (2008).
18. Ilyas, M. et al. Functional divergence of two secreted immune proteases of tomato. *Curr. Biol.* **25**, 2300–2306 (2015).
19. Lozano-Torres, J. L. et al. Dual disease resistance mediated by the immune receptor Cf-2 in tomato requires a common virulence target of a fungus and a nematode. *Proc. Natl Acad. Sci. USA* **109**, 10119–10124 (2012).
20. Mueller, A. N., Ziemann, S., Treitschke, S., Assmann, D. & Doehlemann, G. Compatibility in the *Ustilago maydis*–maize interaction requires inhibition of host cysteine proteases by the fungal effector Pit2. *PLoS Pathog.* **9**, e1003177 (2013).
21. Rooney, H. C. E. Cladosporium Avr2 inhibits tomato Rcr3 protease required for Cf-2-dependent disease resistance. *Science* **308**, 1783–1786 (2005); erratum **310**, 54 (2005).

22. Song, J. et al. Apoplastic effectors secreted by two unrelated eukaryotic plant pathogens target the tomato defense protease Rcr3. *Proc. Natl Acad. Sci. USA* **106**, 1654–1659 (2009).
23. Qi, Z. et al. The syntaxin protein (MoSyn8) mediates intracellular trafficking to regulate conidiogenesis and pathogenicity of rice blast fungus. *New Phytol.* **209**, 1655–1667 (2016).
24. Wang, Y. et al. Comparative secretome investigation of *Magnaporthe oryzae* proteins responsive to nitrogen starvation. *J. Proteome Res.* **10**, 3136–3148 (2011).
25. Talbot, N. J., Ebbole, D. J. & Hamer, J. E. Identification and characterization of Mpg1, a gene involved in pathogenicity from the rice blast fungus *Magnaporthe grisea*. *Plant Cell* **5**, 1575–1590 (1993).
26. Talbot, N. J., McCafferty, H. R. K., Ma, M., Moore, K. & Hamer, J. E. Nitrogen starvation of the rice blast fungus *Magnaporthe grisea* may act as an environmental cue for disease symptom expression. *Physiol. Mol. Plant Pathol.* **50**, 179–195 (1997).
27. Khang, C. H. et al. Translocation of *Magnaporthe oryzae* effectors into rice cells and their subsequent cell-to-cell movement. *Plant Cell* **22**, 1388–1403 (2010).
28. Wu, J. et al. Comparative genomics identifies the *Magnaporthe oryzae* avirulence effector AvrPi9 that triggers Pi9-mediated blast resistance in rice. *New Phytol.* **206**, 1463–1475 (2015).
29. Liu, M. X. et al. Phosphorylation-guarded light-harvesting complex II contributes to broad-spectrum blast resistance in rice. *Proc. Natl Acad. Sci. USA* **116**, 17572–17577 (2019).
30. Mentlak, T. A. et al. Effector-mediated suppression of chitin-triggered immunity by *Magnaporthe oryzae* is necessary for rice blast disease. *Plant Cell* **24**, 322–335 (2012).
31. Hunter, M. S. et al. Selenium single-wavelength anomalous diffraction de novo phasing using an X-ray-free electron laser. *Nat. Commun.* **7**, 13388 (2016).
32. Bendre, A. D., Ramasamy, S. & Suresh, C. G. Analysis of Kunitz inhibitors from plants for comprehensive structural and functional insights. *Int. J. Biol. Macromol.* **113**, 933–943 (2018).
33. Holm, L. & Rosenstrom, P. Dali server: conservation mapping in 3D. *Nucleic Acids Res.* **38**, W545–W549 (2010).
34. Boex-Fontvieille, E., Rustgi, S., von Wettstein, D., Reinbothe, S. & Reinbothe, C. Water-soluble chlorophyll protein is involved in herbivore resistance activation during greening of *Arabidopsis thaliana*. *Proc. Natl Acad. Sci. USA* **112**, 7303–7308 (2015).
35. Rustgi, S., Boex-Fontvieille, E., Reinbothe, C., von Wettstein, D. & Reinbothe, S. Serpin1 and water-soluble chlorophyll protein differentially regulate the activity of the cysteine protease RD21 during plant development in *Arabidopsis thaliana*. *Proc. Natl Acad. Sci. USA* **114**, 2212–2217 (2017).
36. Lampl, N., Alkan, N., Davydov, O. & Fluhr, R. Set-point control of RD21 protease activity by AtSerpin1 controls cell death in *Arabidopsis*. *Plant J.* **74**, 498–510 (2013).
37. Gronnier, J. et al. Structural basis for plant plasma membrane protein dynamics and organization into functional nanodomains. *Elife* **6**, e26404 (2017).
38. Huang, D. Q. et al. Salicylic acid-mediated plasmodesmal closure via Remorin-dependent lipid organization. *Proc. Natl Acad. Sci. USA* **116**, 21274–21284 (2019); erratum **117**, 8659 (2020).
39. Hu, J. et al. Co-evolved plant and blast fungus ascorbate oxidases orchestrate the redox state of host apoplast to modulate rice immunity. *Mol. Plant* **15**, 1347–1366 (2022).
40. Bethune, M. T., Strop, P., Tang, Y. Y., Sollid, L. M. & Khosla, C. Heterologous expression, purification, refolding, and structural-functional characterization of EP-B2, a self-activating barley cysteine endoprotease. *Chem. Biol.* **13**, 637–647 (2006).
41. Comeau, S. R., Gatchell, D. W., Vajda, S. & Camacho, C. J. ClusPro: a fully automated algorithm for protein–protein docking. *Nucleic Acids Res.* **32**, W96–W99 (2004).
42. van der Hoorn, R. A. L., Leeuwenburgh, M. A., Bogyo, M., Joosten, M. H. A. J. & Peck, S. C. Activity profiling of papain-like cysteine proteases in plants. *Plant Physiol.* **135**, 1170–1178 (2004).
43. Chen, T. et al. Diaryl ether: a privileged scaffold for drug and agrochemical discovery. *J. Agric Food Chem.* **68**, 9839–9877 (2020).
44. He, M. et al. Discovery of broad-spectrum fungicides that block septin-dependent infection processes of pathogenic fungi. *Nat. Microbiol.* **5**, 1565–1575 (2020).
45. Zhang, B. et al. PIRIN2 stabilizes cysteine protease XCP2 and increases susceptibility to the vascular pathogen *Ralstonia solanacearum* in *Arabidopsis*. *Plant J.* **79**, 1009–1019 (2014).
46. Lampl, N. et al. *Arabidopsis* AtSerpin1, crystal structure and in vivo interaction with its target protease RESPONSIVE TO DESICCATION-21 (RD21). *J. Biol. Chem.* **285**, 13550–13560 (2010).
47. Halls, C. E. et al. A Kunitz-type cysteine protease inhibitor from cauliflower and *Arabidopsis*. *Plant Sci.* **170**, 1102–1110 (2006).
48. Boex-Fontvieille, E., Rustgi, S., Reinbothe, S. & Reinbothe, C. A Kunitz-type protease inhibitor regulates programmed cell death during flower development in *Arabidopsis thaliana*. *J. Exp. Bot.* **66**, 6119–6135 (2015).
49. Dong, Y. et al. Global genome and transcriptome analyses of *Magnaporthe oryzae* epidemic isolate 98-06 uncover novel effectors and pathogenicity-related genes, revealing gene gain and lose dynamics in genome evolution. *PLoS Pathog.* **11**, e1004801 (2015).
50. Huang, J., Si, W. N., Deng, Q. M., Li, P. & Yang, S. H. Rapid evolution of avirulence genes in rice blast fungus *Magnaporthe oryzae*. *BMC Genet.* **15**, 45 (2014).
51. Liao, J. J. et al. Pathogen effectors and plant immunity determine specialization of the blast fungus to rice subspecies. *Elife* **5**, e19377 (2016).
52. Deb, D., Anderson, R. G., How-Yew-Kin, T., Tyler, B. M. & McDowell, J. M. Conserved RxLR effectors from Oomycetes *Hyaloperonospora arabidopsidis* and *Phytophthora sojae* suppress PAMP- and effector-triggered immunity in diverse plants. *Mol. Plant Microbe* **31**, 374–385 (2018).
53. Thatcher, L. F., Gardiner, D. M., Kazan, K. & Manners, J. M. A highly conserved effector in *Fusarium oxysporum* is required for full virulence on *Arabidopsis*. *Mol. Plant Microbe Interact.* **25**, 180–190 (2012).
54. Xiong, Q. et al. *Phytophthora* suppressor of RNA silencing 2 is a conserved RxLR effector that promotes infection in soybean and *Arabidopsis thaliana*. *Mol. Plant Microbe Interact.* **27**, 1379–1389 (2014).
55. Liu, M. et al. Auxilin-like protein MoSwa2 promotes effector secretion and virulence as a clathrin uncoating factor in the rice blast fungus *Magnaporthe oryzae*. *New Phytol.* **230**, 720–736 (2021).
56. Park, C. H. et al. The *Magnaporthe oryzae* effector AvrPiz-t targets the RING E3 ubiquitin ligase APIP6 to suppress pathogen-associated molecular pattern-triggered immunity in rice. *Plant Cell* **24**, 4748–4762 (2012).
57. Adams, P. D. et al. PHENIX: a comprehensive Python-based system for macromolecular structure solution. *Acta Crystallogr. D* **66**, 213–221 (2010).
58. Emsley, P., Lohkamp, B., Scott, W. G. & Cowtan, K. Features and development of Coot. *Acta Crystallogr. D* **66**, 486–501 (2010).

Acknowledgements

We thank the BL17U1 staff at Shanghai Synchrotron Radiation Facility for data collection and processing, and C. Liao at Nanjing Agricultural University for model colouring. This research was supported by the National Key Research and Development Programme of China (2022YFD1700300), the key programme of the Natural Science

Foundation of China (NSFC) (32030091), NSFC programme 32172377 and NSFC Youth Program 31901832. Research in P.W.'s lab was supported by the US National Institutes of Health under award numbers AI156254 and AI168867.

Author contributions

M.L. and Z.Z. conceived and designed the study. M.L., F.W. and B.H. performed experiments with phenotypic and biochemical assays. M.L., B.H., J.H., Y.D. and W.C. contributed reagents, plant and fungal materials. M.L., F.W., B.H., M.Y., H.Z. and W.X. collected data. M.L., Y.Y., Z.C., X.Z., P.W., W.X. and Z.Z. analysed the data and wrote the paper.

Competing interests

The authors declare no competing interests.

Additional information

Supplementary information The online version contains supplementary material available at https://doi.org/10.1038/s41477-024-01642-x.

Correspondence and requests for materials should be addressed to Weiman Xing or Zhengguang Zhang.

Peer review information *Nature Plants* thanks the anonymous reviewers for their contribution to the peer review of this work.

nature portfolio

Corresponding author(s): Zhengguang Zhang

Last updated by author(s): 23/01/2024

Reporting Summary

Nature Portfolio wishes to improve the reproducibility of the work that we publish. This form provides structure for consistency and transparency in reporting. For further information on Nature Portfolio policies, see our Editorial Policies and the Editorial Policy Checklist.

Statistics

For all statistical analyses, confirm that the following items are present in the figure legend, table legend, main text, or Methods section.

n/a	Confirmed	
☐	☒	The exact sample size (*n*) for each experimental group/condition, given as a discrete number and unit of measurement
☐	☒	A statement on whether measurements were taken from distinct samples or whether the same sample was measured repeatedly
☐	☒	The statistical test(s) used AND whether they are one- or two-sided *Only common tests should be described solely by name; describe more complex techniques in the Methods section.*
☒	☐	A description of all covariates tested
☐	☒	A description of any assumptions or corrections, such as tests of normality and adjustment for multiple comparisons
☐	☒	A full description of the statistical parameters including central tendency (e.g. means) or other basic estimates (e.g. regression coefficient) AND variation (e.g. standard deviation) or associated estimates of uncertainty (e.g. confidence intervals)
☐	☒	For null hypothesis testing, the test statistic (e.g. *F*, *t*, *r*) with confidence intervals, effect sizes, degrees of freedom and *P* value noted *Give P values as exact values whenever suitable.*
☒	☐	For Bayesian analysis, information on the choice of priors and Markov chain Monte Carlo settings
☒	☐	For hierarchical and complex designs, identification of the appropriate level for tests and full reporting of outcomes
☒	☐	Estimates of effect sizes (e.g. Cohen's *d*, Pearson's *r*), indicating how they were calculated

Our web collection on statistics for biologists contains articles on many of the points above.

Software and code

Policy information about availability of computer code

Data collection	Images from Immuno Blotting, DNA gel and co-immunoprecipitation were collected with image Lab (Bio-Rad, version 7.2.0) Confocal images were collected with ZEISS LSM710 (ZEN 2010 black version) All of the structure-related pictures in this research were collected using PyMOL (version 2.1.0)
Data analysis	qRT-PCR was performed with the ABI 7500 Fast Real-Time System and transcripts were analyzed by the 7500 System SDS software v1.3.1 The data of Microscale Thermophoresis (MST) analysis were collected with the Nano Temper Analysis Software (Version 1.5.41) HKL2000/3000 package (HKL Research Inc., Charlottesville, VA, USA) The protein structural data were analysed by the Phenix software (version 1.4) The data of synthetic compounds were analysed by JEOL ECX-500 (Delta NMR Software and MestReNova 14.0) Data Processing System v18.10 and Microsoft Excel 2019 were used for statistical analysis and graphs data presentation

For manuscripts utilizing custom algorithms or software that are central to the research but not yet described in published literature, software must be made available to editors and reviewers. We strongly encourage code deposition in a community repository (e.g. GitHub). See the Nature Portfolio guidelines for submitting code & software for further information.

Data

Policy information about availability of data

All manuscripts must include a data availability statement. This statement should provide the following information, where applicable:

- Accession codes, unique identifiers, or web links for publicly available datasets
- A description of any restrictions on data availability
- For clinical datasets or third party data, please ensure that the statement adheres to our policy

All data generated or analyzed during this study were included in this published article and supplementary files. Bio-reagents are available for research propose upon request from the corresponding author under a material transfer agreement. The accessible link of NCBI Non-redundant protein sequences (nr) databases is https://blast.ncbi.nlm.nih.gov/Blast.cgi.

Research involving human participants, their data, or biological material

Policy information about studies with human participants or human data. See also policy information about sex, gender (identity/presentation), and sexual orientation and race, ethnicity and racism.

Reporting on sex and gender	N/A
Reporting on race, ethnicity, or other socially relevant groupings	N/A
Population characteristics	N/A
Recruitment	N/A
Ethics oversight	N/A

Note that full information on the approval of the study protocol must also be provided in the manuscript.

Field-specific reporting

Please select the one below that is the best fit for your research. If you are not sure, read the appropriate sections before making your selection.

☒ Life sciences ☐ Behavioural & social sciences ☐ Ecological, evolutionary & environmental sciences

For a reference copy of the document with all sections, see nature.com/documents/nr-reporting-summary-flat.pdf

Life sciences study design

All studies must disclose on these points even when the disclosure is negative.

Sample size	Sample sizes were determined according to similar studied in the field. Reference: Muxing L, Suobing Z, Jiexiong H et al., Phosphorylation-guarded light-harvesting complex II contributes to broad-spectrum blast resistance in rice. P Natl Acad Sci USA 116, 17572-17577 (2019). Sample sizes were also determined by previous pilot experiments to be sufficient to achieve desired outcomes. Sample sizes are indicated in the Figures, legends and main text.
Data exclusions	No data were excluded from the analysis.
Replication	All experimental findings were reproduced in several independent biological experiments (n) with multiple technical replicates. The number of repeats is indicated in the figures and figure legends. All attempts to replicate the experiments were successful and approved by multiple researchers.
Randomization	Samples of the same genotypes and growth conditions were randomly collected and pooled for downstream experiments.
Blinding	Investigators were not blinded to plant-pathogen genotypes during experiments. The research materials are plants and pathogens so the blinding design is not applicable to this system. Experiment results are not subjective.

Behavioural & social sciences study design

All studies must disclose on these points even when the disclosure is negative.

Study description	*Briefly describe the study type including whether data are quantitative, qualitative, or mixed-methods (e.g. qualitative cross-sectional,*

Study description	*quantitative experimental, mixed-methods case study).*
Research sample	*State the research sample (e.g. Harvard university undergraduates, villagers in rural India) and provide relevant demographic information (e.g. age, sex) and indicate whether the sample is representative. Provide a rationale for the study sample chosen. For studies involving existing datasets, please describe the dataset and source.*
Sampling strategy	*Describe the sampling procedure (e.g. random, snowball, stratified, convenience). Describe the statistical methods that were used to predetermine sample size OR if no sample-size calculation was performed, describe how sample sizes were chosen and provide a rationale for why these sample sizes are sufficient. For qualitative data, please indicate whether data saturation was considered, and what criteria were used to decide that no further sampling was needed.*
Data collection	*Provide details about the data collection procedure, including the instruments or devices used to record the data (e.g. pen and paper, computer, eye tracker, video or audio equipment) whether anyone was present besides the participant(s) and the researcher, and whether the researcher was blind to experimental condition and/or the study hypothesis during data collection.*
Timing	*Indicate the start and stop dates of data collection. If there is a gap between collection periods, state the dates for each sample cohort.*
Data exclusions	*If no data were excluded from the analyses, state so OR if data were excluded, provide the exact number of exclusions and the rationale behind them, indicating whether exclusion criteria were pre-established.*
Non-participation	*State how many participants dropped out/declined participation and the reason(s) given OR provide response rate OR state that no participants dropped out/declined participation.*
Randomization	*If participants were not allocated into experimental groups, state so OR describe how participants were allocated to groups, and if allocation was not random, describe how covariates were controlled.*

Ecological, evolutionary & environmental sciences study design

All studies must disclose on these points even when the disclosure is negative.

Study description	*Briefly describe the study. For quantitative data include treatment factors and interactions, design structure (e.g. factorial, nested, hierarchical), nature and number of experimental units and replicates.*
Research sample	*Describe the research sample (e.g. a group of tagged Passer domesticus, all Stenocereus thurberi within Organ Pipe Cactus National Monument), and provide a rationale for the sample choice. When relevant, describe the organism taxa, source, sex, age range and any manipulations. State what population the sample is meant to represent when applicable. For studies involving existing datasets, describe the data and its source.*
Sampling strategy	*Note the sampling procedure. Describe the statistical methods that were used to predetermine sample size OR if no sample-size calculation was performed, describe how sample sizes were chosen and provide a rationale for why these sample sizes are sufficient.*
Data collection	*Describe the data collection procedure, including who recorded the data and how.*
Timing and spatial scale	*Indicate the start and stop dates of data collection, noting the frequency and periodicity of sampling and providing a rationale for these choices. If there is a gap between collection periods, state the dates for each sample cohort. Specify the spatial scale from which the data are taken*
Data exclusions	*If no data were excluded from the analyses, state so OR if data were excluded, describe the exclusions and the rationale behind them, indicating whether exclusion criteria were pre-established.*
Reproducibility	*Describe the measures taken to verify the reproducibility of experimental findings. For each experiment, note whether any attempts to repeat the experiment failed OR state that all attempts to repeat the experiment were successful.*
Randomization	*Describe how samples/organisms/participants were allocated into groups. If allocation was not random, describe how covariates were controlled. If this is not relevant to your study, explain why.*
Blinding	*Describe the extent of blinding used during data acquisition and analysis. If blinding was not possible, describe why OR explain why blinding was not relevant to your study.*

Did the study involve field work? ☐ Yes ☐ No

Field work, collection and transport

Field conditions	*Describe the study conditions for field work, providing relevant parameters (e.g. temperature, rainfall).*
Location	*State the location of the sampling or experiment, providing relevant parameters (e.g. latitude and longitude, elevation, water depth).*
Access & import/export	*Describe the efforts you have made to access habitats and to collect and import/export your samples in a responsible manner and in*

Access & import/export	*compliance with local, national and international laws, noting any permits that were obtained (give the name of the issuing authority, the date of issue, and any identifying information).*
Disturbance	*Describe any disturbance caused by the study and how it was minimized.*

Reporting for specific materials, systems and methods

We require information from authors about some types of materials, experimental systems and methods used in many studies. Here, indicate whether each material, system or method listed is relevant to your study. If you are not sure if a list item applies to your research, read the appropriate section before selecting a response.

Materials & experimental systems

n/a	Involved in the study
☐	☒ Antibodies
☒	☐ Eukaryotic cell lines
☒	☐ Palaeontology and archaeology
☒	☐ Animals and other organisms
☒	☐ Clinical data
☒	☐ Dual use research of concern
☐	☒ Plants

Methods

n/a	Involved in the study
☒	☐ ChIP-seq
☒	☐ Flow cytometry
☒	☐ MRI-based neuroimaging

Antibodies

Antibodies used	Anti-Flag Antibody (Provided by Engibody, catalog number AT0022) Anti-GFP Antibody (Provided by Abmart, catalog number M20004) Anti-GST Antibody (Provided by Abmart , catalog number M20007L) Anti-RFP Antibody (Provided by Abbkine , catalog numberA02120) Streptavidin-HRP Antibody (Provided by Abcam , catalog number ab7403)
Validation	The above commercial antibodies have been validated for Immunoprecipitation and Western Blot in the several published papers and used for co-immunoprecipitation and Enzyme activity determination in this study. The validation statements can be found at product websites: Anti-Flag Antibody: https://www.engibody.com/catalog/search.aspx?k=AT0022 Anti-GFP Antibody: https://www.ab-mart.com.cn/page.aspx?node=%2059%20&id=%20971 Anti-GST Antibody: https://www.ab-mart.com.cn/page.aspx?node=%2059%20&id=%20967 Anti-RFP Antibody: https://www.abbkine.com/product/anti-rfp-tag-mouse-monoclonal-antibody-9d1-abt2120/ Streptavidin-HRP Antibody: https://www.abcam.cn/products/proteins-peptides/streptavidin-hrp-ab7403.html

Eukaryotic cell lines

Policy information about cell lines and Sex and Gender in Research

Cell line source(s)	*State the source of each cell line used and the sex of all primary cell lines and cells derived from human participants or vertebrate models.*
Authentication	*Describe the authentication procedures for each cell line used OR declare that none of the cell lines used were authenticated.*
Mycoplasma contamination	*Confirm that all cell lines tested negative for mycoplasma contamination OR describe the results of the testing for mycoplasma contamination OR declare that the cell lines were not tested for mycoplasma contamination.*
Commonly misidentified lines (See ICLAC register)	*Name any commonly misidentified cell lines used in the study and provide a rationale for their use.*

Palaeontology and Archaeology

Specimen provenance	*Provide provenance information for specimens and describe permits that were obtained for the work (including the name of the issuing authority, the date of issue, and any identifying information). Permits should encompass collection and, where applicable, export.*
Specimen deposition	*Indicate where the specimens have been deposited to permit free access by other researchers.*

Dating methods	*If new dates are provided, describe how they were obtained (e.g. collection, storage, sample pretreatment and measurement), where they were obtained (i.e. lab name), the calibration program and the protocol for quality assurance OR state that no new dates are provided.*

☐ Tick this box to confirm that the raw and calibrated dates are available in the paper or in Supplementary Information.

Ethics oversight	*Identify the organization(s) that approved or provided guidance on the study protocol, OR state that no ethical approval or guidance was required and explain why not.*

Note that full information on the approval of the study protocol must also be provided in the manuscript.

Animals and other research organisms

Policy information about studies involving animals; ARRIVE guidelines recommended for reporting animal research, and Sex and Gender in Research

Laboratory animals	*For laboratory animals, report species, strain and age OR state that the study did not involve laboratory animals.*
Wild animals	*Provide details on animals observed in or captured in the field; report species and age where possible. Describe how animals were caught and transported and what happened to captive animals after the study (if killed, explain why and describe method; if released, say where and when) OR state that the study did not involve wild animals.*
Reporting on sex	*Indicate if findings apply to only one sex; describe whether sex was considered in study design, methods used for assigning sex. Provide data disaggregated for sex where this information has been collected in the source data as appropriate; provide overall numbers in this Reporting Summary. Please state if this information has not been collected. Report sex-based analyses where performed, justify reasons for lack of sex-based analysis.*
Field-collected samples	*For laboratory work with field-collected samples, describe all relevant parameters such as housing, maintenance, temperature, photoperiod and end-of-experiment protocol OR state that the study did not involve samples collected from the field.*
Ethics oversight	*Identify the organization(s) that approved or provided guidance on the study protocol, OR state that no ethical approval or guidance was required and explain why not.*

Note that full information on the approval of the study protocol must also be provided in the manuscript.

Clinical data

Policy information about clinical studies

All manuscripts should comply with the ICMJE guidelines for publication of clinical research and a completed CONSORT checklist must be included with all submissions.

Clinical trial registration	*Provide the trial registration number from ClinicalTrials.gov or an equivalent agency.*
Study protocol	*Note where the full trial protocol can be accessed OR if not available, explain why.*
Data collection	*Describe the settings and locales of data collection, noting the time periods of recruitment and data collection.*
Outcomes	*Describe how you pre-defined primary and secondary outcome measures and how you assessed these measures.*

Dual use research of concern

Policy information about dual use research of concern

Hazards

Could the accidental, deliberate or reckless misuse of agents or technologies generated in the work, or the application of information presented in the manuscript, pose a threat to:

No	Yes	
☒	☐	Public health
☒	☐	National security
☒	☐	Crops and/or livestock
☒	☐	Ecosystems
☒	☐	Any other significant area

Experiments of concern

Does the work involve any of these experiments of concern:

No	Yes	
☒	☐	Demonstrate how to render a vaccine ineffective
☒	☐	Confer resistance to therapeutically useful antibiotics or antiviral agents
☒	☐	Enhance the virulence of a pathogen or render a nonpathogen virulent
☒	☐	Increase transmissibility of a pathogen
☒	☐	Alter the host range of a pathogen
☒	☐	Enable evasion of diagnostic/detection modalities
☒	☐	Enable the weaponization of a biological agent or toxin
☒	☐	Any other potentially harmful combination of experiments and agents

Plants

Seed stocks

Report on the source of all seed stocks or other plant material used. If applicable, state the seed stock centre and catalogue number. If plant specimens were collected from the field, describe the collection location, date and sampling procedures.

Novel plant genotypes

Describe the methods by which all novel plant genotypes were produced. This includes those generated by transgenic approaches, gene editing, chemical/radiation-based mutagenesis and hybridization. For transgenic lines, describe the transformation method, the number of independent lines analyzed and the generation upon which experiments were performed. For gene-edited lines, describe the editor used, the endogenous sequence targeted for editing, the targeting guide RNA sequence (if applicable) and how the editor was applied.

Authentication

Describe any authentication procedures for each seed stock used or novel genotype generated. Describe any experiments used to assess the effect of a mutation and, where applicable, how potential secondary effects (e.g. second site T-DNA insertions, mosiacism, off-target gene editing) were examined.

ChIP-seq

Data deposition

☐ Confirm that both raw and final processed data have been deposited in a public database such as GEO.

☐ Confirm that you have deposited or provided access to graph files (e.g. BED files) for the called peaks.

Data access links
May remain private before publication.

For "Initial submission" or "Revised version" documents, provide reviewer access links. For your "Final submission" document, provide a link to the deposited data.

Files in database submission

Provide a list of all files available in the database submission.

Genome browser session
(e.g. UCSC)

Provide a link to an anonymized genome browser session for "Initial submission" and "Revised version" documents only, to enable peer review. Write "no longer applicable" for "Final submission" documents.

Methodology

Replicates

Describe the experimental replicates, specifying number, type and replicate agreement.

Sequencing depth

Describe the sequencing depth for each experiment, providing the total number of reads, uniquely mapped reads, length of reads and whether they were paired- or single-end.

Antibodies

Describe the antibodies used for the ChIP-seq experiments; as applicable, provide supplier name, catalog number, clone name, and lot number.

Peak calling parameters

Specify the command line program and parameters used for read mapping and peak calling, including the ChIP, control and index files used.

Data quality

Describe the methods used to ensure data quality in full detail, including how many peaks are at FDR 5% and above 5-fold enrichment.

Software

Describe the software used to collect and analyze the ChIP-seq data. For custom code that has been deposited into a community repository, provide accession details.

Flow Cytometry

Plots

Confirm that:

☐ The axis labels state the marker and fluorochrome used (e.g. CD4-FITC).

☐ The axis scales are clearly visible. Include numbers along axes only for bottom left plot of group (a 'group' is an analysis of identical markers).

☐ All plots are contour plots with outliers or pseudocolor plots.

☐ A numerical value for number of cells or percentage (with statistics) is provided.

Methodology

Sample preparation	*Describe the sample preparation, detailing the biological source of the cells and any tissue processing steps used.*
Instrument	*Identify the instrument used for data collection, specifying make and model number.*
Software	*Describe the software used to collect and analyze the flow cytometry data. For custom code that has been deposited into a community repository, provide accession details.*
Cell population abundance	*Describe the abundance of the relevant cell populations within post-sort fractions, providing details on the purity of the samples and how it was determined.*
Gating strategy	*Describe the gating strategy used for all relevant experiments, specifying the preliminary FSC/SSC gates of the starting cell population, indicating where boundaries between "positive" and "negative" staining cell populations are defined.*

☐ Tick this box to confirm that a figure exemplifying the gating strategy is provided in the Supplementary Information.

Magnetic resonance imaging

Experimental design

Design type	*Indicate task or resting state; event-related or block design.*
Design specifications	*Specify the number of blocks, trials or experimental units per session and/or subject, and specify the length of each trial or block (if trials are blocked) and interval between trials.*
Behavioral performance measures	*State number and/or type of variables recorded (e.g. correct button press, response time) and what statistics were used to establish that the subjects were performing the task as expected (e.g. mean, range, and/or standard deviation across subjects).*

Acquisition

Imaging type(s)	*Specify: functional, structural, diffusion, perfusion.*
Field strength	*Specify in Tesla*
Sequence & imaging parameters	*Specify the pulse sequence type (gradient echo, spin echo, etc.), imaging type (EPI, spiral, etc.), field of view, matrix size, slice thickness, orientation and TE/TR/flip angle.*
Area of acquisition	*State whether a whole brain scan was used OR define the area of acquisition, describing how the region was determined.*

Diffusion MRI ☐ Used ☐ Not used

Preprocessing

Preprocessing software	*Provide detail on software version and revision number and on specific parameters (model/functions, brain extraction, segmentation, smoothing kernel size, etc.).*
Normalization	*If data were normalized/standardized, describe the approach(es): specify linear or non-linear and define image types used for transformation OR indicate that data were not normalized and explain rationale for lack of normalization.*
Normalization template	*Describe the template used for normalization/transformation, specifying subject space or group standardized space (e.g. original Talairach, MNI305, ICBM152) OR indicate that the data were not normalized.*
Noise and artifact removal	*Describe your procedure(s) for artifact and structured noise removal, specifying motion parameters, tissue signals and physiological signals (heart rate, respiration).*

Volume censoring

Define your software and/or method and criteria for volume censoring, and state the extent of such censoring.

Statistical modeling & inference

Model type and settings

Specify type (mass univariate, multivariate, RSA, predictive, etc.) and describe essential details of the model at the first and second levels (e.g. fixed, random or mixed effects; drift or auto-correlation).

Effect(s) tested

Define precise effect in terms of the task or stimulus conditions instead of psychological concepts and indicate whether ANOVA or factorial designs were used.

Specify type of analysis: ☐ Whole brain ☐ ROI-based ☐ Both

Statistic type for inference

Specify voxel-wise or cluster-wise and report all relevant parameters for cluster-wise methods.

(See Eklund et al. 2016)

Correction

Describe the type of correction and how it is obtained for multiple comparisons (e.g. FWE, FDR, permutation or Monte Carlo).

Models & analysis

n/a	Involved in the study
☐	☐ Functional and/or effective connectivity
☐	☐ Graph analysis
☐	☐ Multivariate modeling or predictive analysis

Functional and/or effective connectivity

Report the measures of dependence used and the model details (e.g. Pearson correlation, partial correlation, mutual information).

Graph analysis

Report the dependent variable and connectivity measure, specifying weighted graph or binarized graph, subject- or group-level, and the global and/or node summaries used (e.g. clustering coefficient, efficiency, etc.).

Multivariate modeling and predictive analysis

Specify independent variables, features extraction and dimension reduction, model, training and evaluation metrics.